Portable Pipe Mapper (PPM) Field Test at the Idaho Chemical Processing Plant (ICPP)

Report Prepared
by
Dr. Ben Motazed

Field Robotics Center
Robotics Institute
Carnegie Mellon University
Pittsburgh, PA 15213
(412) 268-6550

January 1992

Acknowledgments

The author likes to thank Miss Lori Martinson, Mr. Chuck Urbanski, Mr. Lou Hong and Mr. Darin Wells at WINCO for their assistance and patience in creating this opportunity for the Portable Pipe Mapper Technology to be demonstrated at Idaho National laboratories.

Without Mr. Bryon Smith, Mr. David White and Mr. Jim Martin representing the personnel at Carnegie Mellon University, none of this work could have been possible. My deepest appreciation for their continued support and dedication.

Introduction

This document reports on the investigation conducted by Carnegie Mellon University (CMU) researchers at Idaho National Laboratories (INEL) to demonstrate the potential of the Portable Pipe Mapper (PPM) system for mapping buried pipes at the ICPP facility.

The investigation was conducted in two phases; the first phase addressed the data acquisition at the ICPP site in September of '91, and the second phase focused on data processing/analysis and reporting at CMU. During the three day period at INEL, a total of ten complete pipe maps, covering three separate sites, were collected as shown below:

Site	No. of Maps Made	Map ID Numbers
Beech Street	2	01-0927, 02-0927
Olive Avenue	1	03-0927
Cedar Street	7	01...07-0930

In each case, the map was intended to identify and locate a specific buried pipe line, both in plan and depth from the ground surface. In almost all cases, it was possible to determine the depth of buried lines with reasonable confidence. In some cases, the magnetic maps identified additional buried lines, i.e. ones which were not indicated in ICPP blueprints.

This report is organized in three parts. In part one, a brief explanation is given about the PPM's operation, data acquisition, and the processing schemes used to develop pipe maps. In part two, results of this investigation are explained in detail for each site. In part three, all digitized magnetic maps, and related field vectors for depth determination are presented for further insight into each case.

Part I. Data Acquisition and Depth Determination

Buried pipe mapping is based on the acquisition of position tagged 3D magnetic field vector measurements made on the ground surface using the PPM. In this manner a map, or an image of the magnetic field activity emanating from the ground can be displayed and retained for further analysis. At INEL, the PPM was equipped with an encoder wheel as a position tagging device. As the crew pushed the PPM, an internal sensor measured the magnitude of all three magnetic field components emanating from the ground at regular intervals. The magnetic field was introduced in the buried pipes by transmitting an AC signal via direct coupling to an exposed part of the pipe.

The PPM sensor simultaneously measures the three principal components of the magnetic field, namely X, Y & Z. The X & Y components are parallel to the plane of scan, and normal to each other. The Z component is the vertical component, normal to the plane of scan. By convention a map has an origin that defines the Cartesian coordinates for the X, Y & Z magnetic field components. The PPM sensor also measures the relative phase difference between the X, Y & Z signals and the transmitted signal. This information is later used to assign a positive or negative sign to each of the three components (Grey scale representations of magnitude variation of X, Y, Z components and associated phase are in part three of this report for all of the ten maps acquired at INEL (fig. 11-30). In these images, bright pixels represent high signal intensity). The X & Y

field components are of largest magnitude if they are normal to and directly above the long axis of a pipe, and of smallest magnitude if they are parallel to it. The Z component is invariant to the direction of a pipe; it is always at a minimum almost directly above a pipe, largest away from the pipe, and attenuates as a function of distance. Invariance of Z axis component measurements to pipe direction and acute minimum response directly above a pipe is a powerful means to make initial estimates for identifying pipes in a Z component image. Through out the remainder of this report, only processed (minimum signal marked) Z-axis images are used to convey pipe outlines.

The vector sum of X, Y, Z field component magnitudes define the magnitude of field vectors, where as their relative intensity (directional cosines) define the direction of field vectors. The resultant information about magnitude and direction of magnetic field vectors is then used to estimate depth of the field source. Each field vector is tangential to an equipotential field, sourced at a buried pipe. In an ideal situation (single pipe, no interference), orthogonal lines from a group of field vectors along a *sample line* normal to the axis of a pipe, are theoretically coincident at the source of the field, (i.e. the pipe). Using the length of a sample line as a linear scale, and relative inclination of orthogonal vectors, it is a simple matter to calculate the depth at which all orthogonal vectors are coincident. Of course, as the data in this report illustrate, field measurements are always far from ideal, and the lines rarely intersect at a single point. Instead there is a distribution of intersection points that are concentrated near the (ideal) single point. This concept is graphically shown in figure 1. For sake of clarity, in this document, the common intersection points are labelled as squares throughout all the figures showing the pipes in the plane and cross-section.

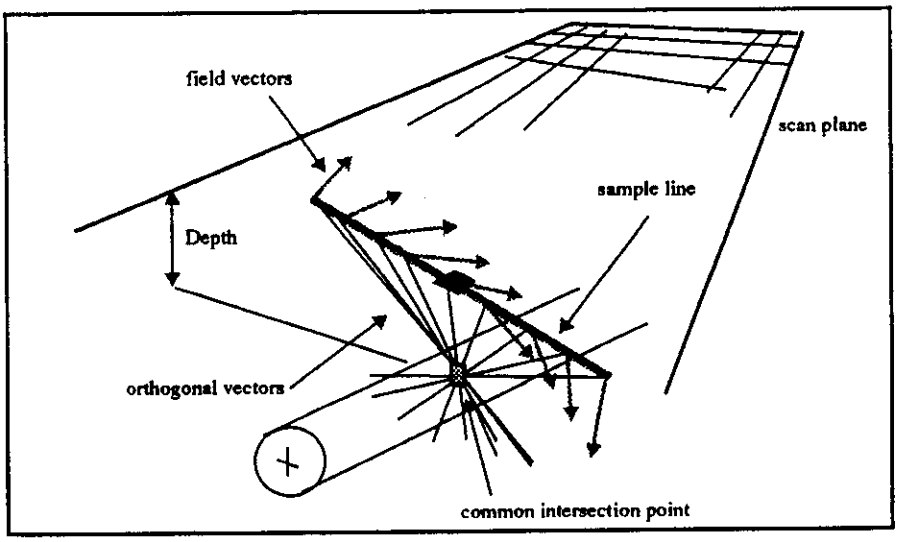

Figure 1. Orthogonal Vectors of Field Vectors Coincident at a Point

Part II. Results

Beech Street

At this site it was necessary to determine the depth of two lines, 1.5" PWA-1561 & 2" PWA-1560. Both lines exit valve box DVB-YDA-PL-C33 as shown in figure 2. The first map (01-0927, 64'x40') covers the section where the two pipes make a 90 degree turn, and the second map (02-0927, 40'x32') covers pipe extensions adjacent to valve box DVB-YDA-SW-D12. Figure3 shows the vertical component of the magnetic field for both maps. In these maps the darkest linear regions identify a pipe, for the vertical component is nearly zero above the pipes. The bright area enclosed by the bend is the region where the vertical components from each leg of the bend reinforce each other, and therefore produce the largest magnitude. In contrast, the opposite side of the bend experiences the least reinforcement, and therefore appears dark. Also, due to the close proximity of pipes in relation to their considerable depth, the magnetic features at the surface show the presence of one large pipe, rather then two separate pipes. As shown in figure 4, within map 01-0927, the depth of the pipes near valve box DVB-YDA-PL-C33 is about 13', changing quickly to 11', and then gradually rising to 7' at the end of the bend. It is therefore reasonable to claim that the pipes are not really deeper than 11'. This fact can further be verified by directly measuring the depth of pipes from the surface at the valve box man-hole.

Unfortunately the signal from the pipes is not evident in map 02-0927. This may be attributed to a some magnetic distortion, or simply an error in the mapping process, where the map did not cover the area above the pipes. However, a pipe feature is clearly present at the average depth of 8.4' (figure 4). In this map the bright area is again associated with the reinforcing of the vertical magnetic components at the bend of the lines entering valve box DVB-YDA-SW-D12.

Olive Avenue

A single map was produced near Olive Avenue in front of building 633 to verify the presence of a large stainless steel valve box in the middle of the map. A detailed plan of the site was not available at time of the reporting to match against the magnetic maps. As seen in figure 5. the large and wide dark regions associated with the vertical component of the field indicate a broad field emanating deep from the subsurface. Figure 5 further shows the long sample lines used to a estimate moderately deep (7.5', 5.63') and very deep sources (21.25', 25').

Cedar Street

The objective of mapping Cedar Street between CPP-654 & CPP-664 was to determine the depth of the 4" water line CWNR-110865 (figure 6). At this site, a total of 7 maps were collected. Although the images are not to scale with the original blueprints, a composite made by assembling the vertical component images end to end (figure 7) reveals all of the buried lines expected to be seen at this site, namely the desired CWNR-110865, the crossing telephone line and 1" ADT Conduit, 24KV Power Line, as well as a conduit at the approximate depth of 5' not shown in the plans within map 01-0930. Since the PPM electromagnetic signal was directly attached to CWNR-110865, its depth can reliably be estimated to be 6' (map 01-0930), gradually rising to 5.5' (map 07-0930). Consistent depth estimates for the other conduits evident in the images were not obtained; this is likely due to their fields been the result of secondary coupling to CWNR-110865 (which was directly energized). For certainty it is necessary to directly couple to these conduits and verify the current results. Figures 8, 9 & 10 show depth estimates along sample

lines in all of the 7 maps on Cedar Street.

Part III. Additional Data

Part III of this report starting at figure 11, contains ten pairs of figures (total of 20) for each of the ten maps acquired at ICPP.

In each pair of figures, the first figure shows the raw X, Y & Z magnitude/phase maps, the composite map (grey scale representation of field vector magnitudes), and sampled line diagram to serve as a guide for matching field & depth vector diagrams that follow in the second figure. In the first figure note the sudden shift in phase intensity from one side of a pipe to another in the Z-axis component map, that signify the change in sign of the Z field component as it crosses over the long axis of a pipe.

The second figure in the pair, shows as many as six vector intersection diagrams, each numbered according to the sampled line number from the previous figure. Aside from determining depth of common intersection point of orthogonal line, these diagrams rank the confidence level for a depth value. The confidence level is governed by the number of coincident orthogonal lines, and the sampled line's inclination angle with the pipe outline. For example, in case 01-0927, sampled lines #5 & #6 are more perpendicular to the pipe outline as compared to sampled line #4. Although intersection points for all three cases seem to be tightly distributed, however the depth value from case #5 & #6 seem more consistent at 7', rather than 7.62' from sampled line #4.

Conclusions

The demonstration of PPM at ICPP sets a major precedence in proving the effectiveness of magnetic mapping versus point measurements by conventional pipe locators. Additionally, the availability of uncommon data from this investigation enabled further development of capabilities and potential of data processing and depth determination algorithms. Aside from the case at Olive Street, which lacked clear magnetic features from a pipe, and map 02-0927 at Beech Street that seemed inconsistent with the blueprints and the adjacent map, overall PPM performance met expectations in effectively characterizing the subsurface infrastructure at ICPP.

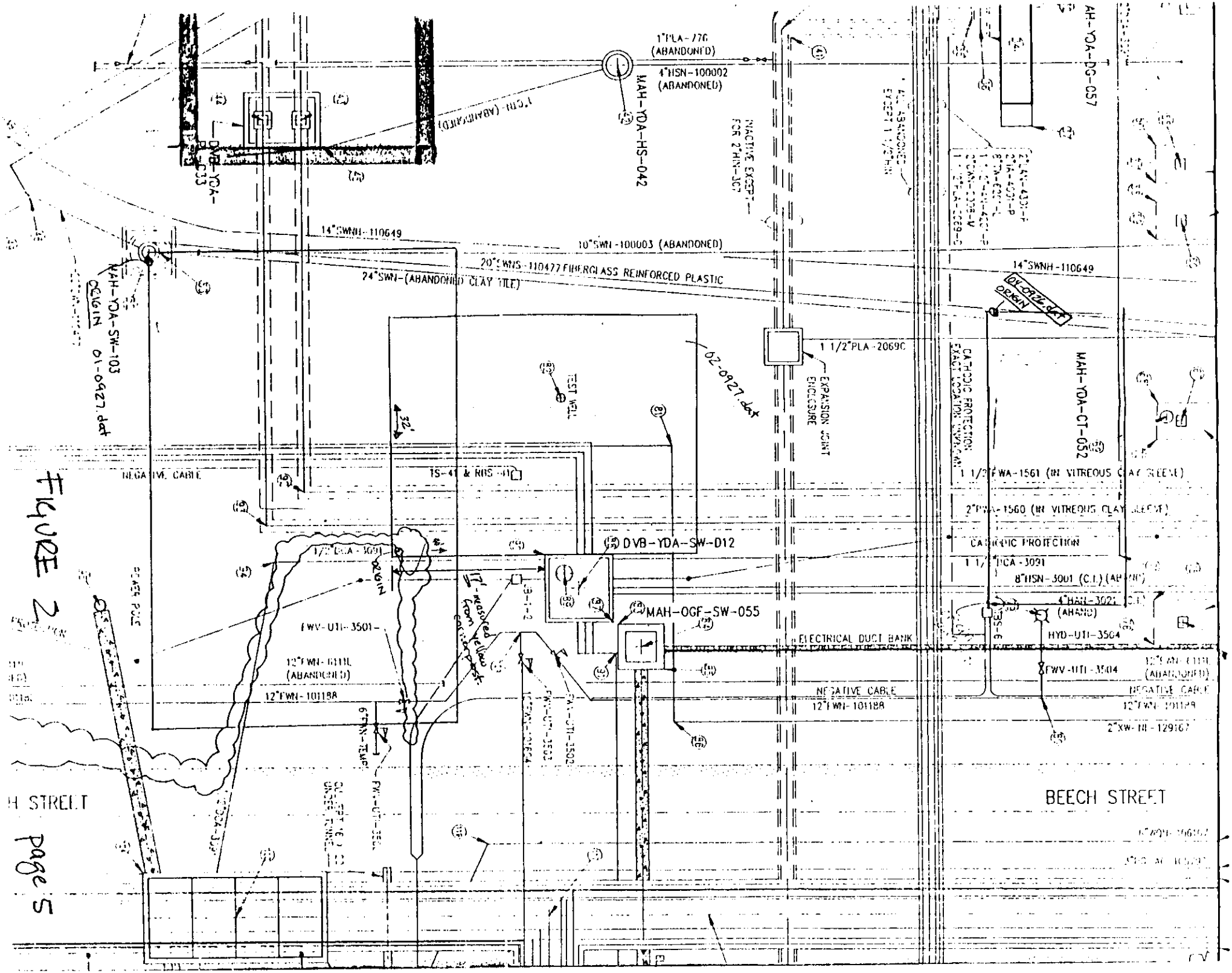

FIGURE 2

Page 5

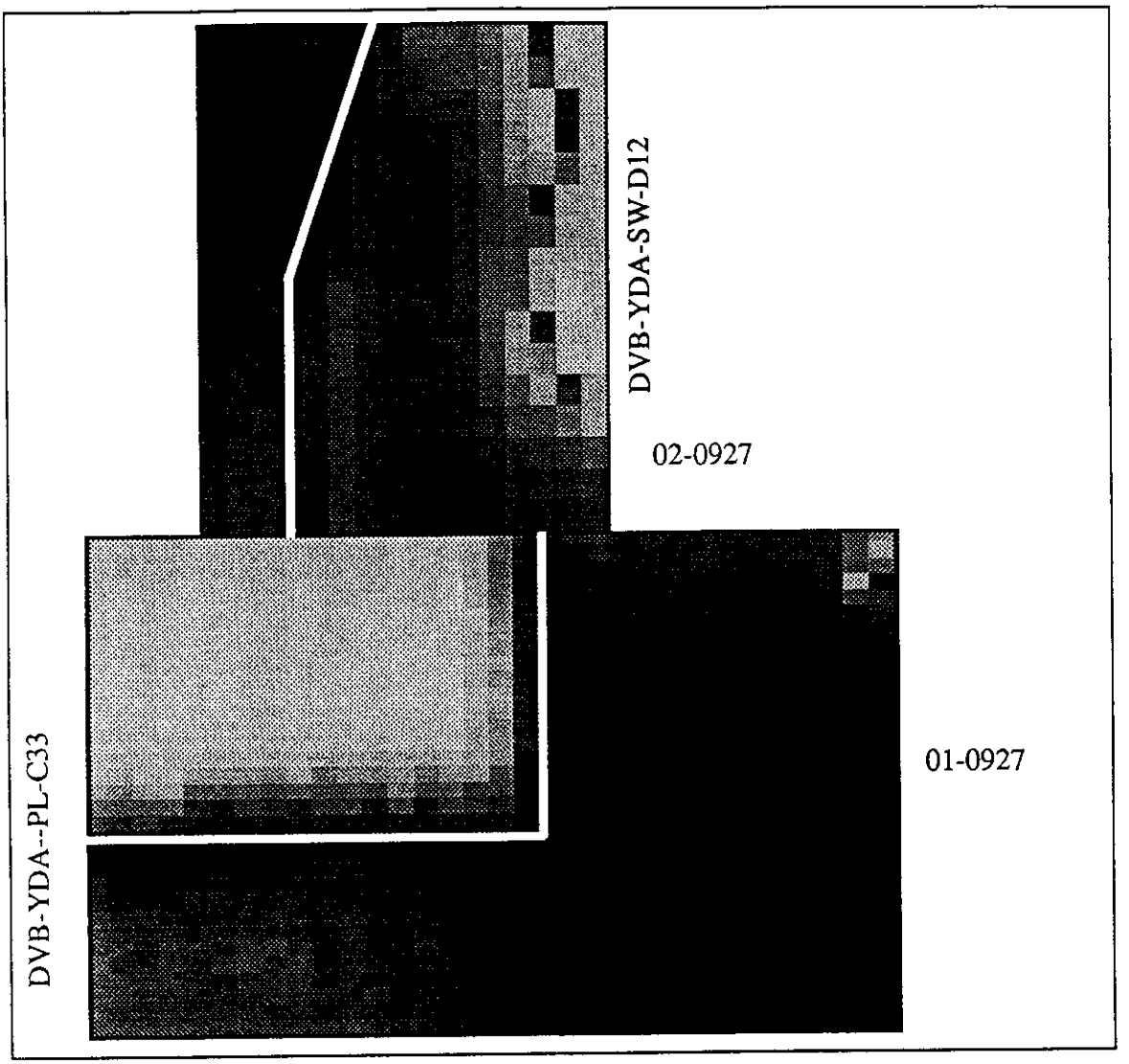

Figure 3. Beech Street Site

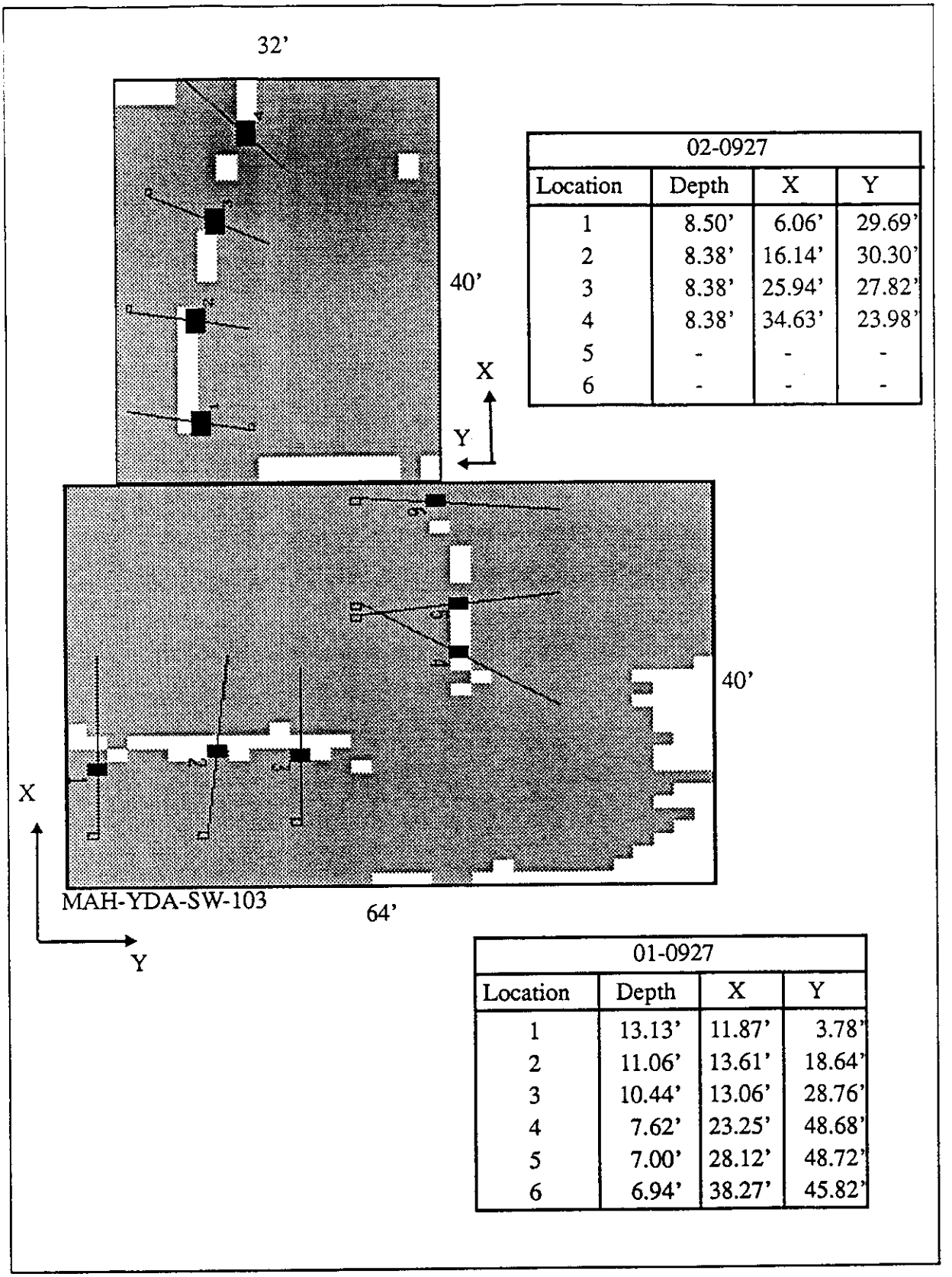

02-0927			
Location	Depth	X	Y
1	8.50'	6.06'	29.69'
2	8.38'	16.14'	30.30'
3	8.38'	25.94'	27.82'
4	8.38'	34.63'	23.98'
5	-	-	-
6	-	-	-

01-0927			
Location	Depth	X	Y
1	13.13'	11.87'	3.78'
2	11.06'	13.61'	18.64'
3	10.44'	13.06'	28.76'
4	7.62'	23.25'	48.68'
5	7.00'	28.12'	48.72'
6	6.94'	38.27'	45.82'

Figure 4. Maps 1 & 2 at the Beech Street Site

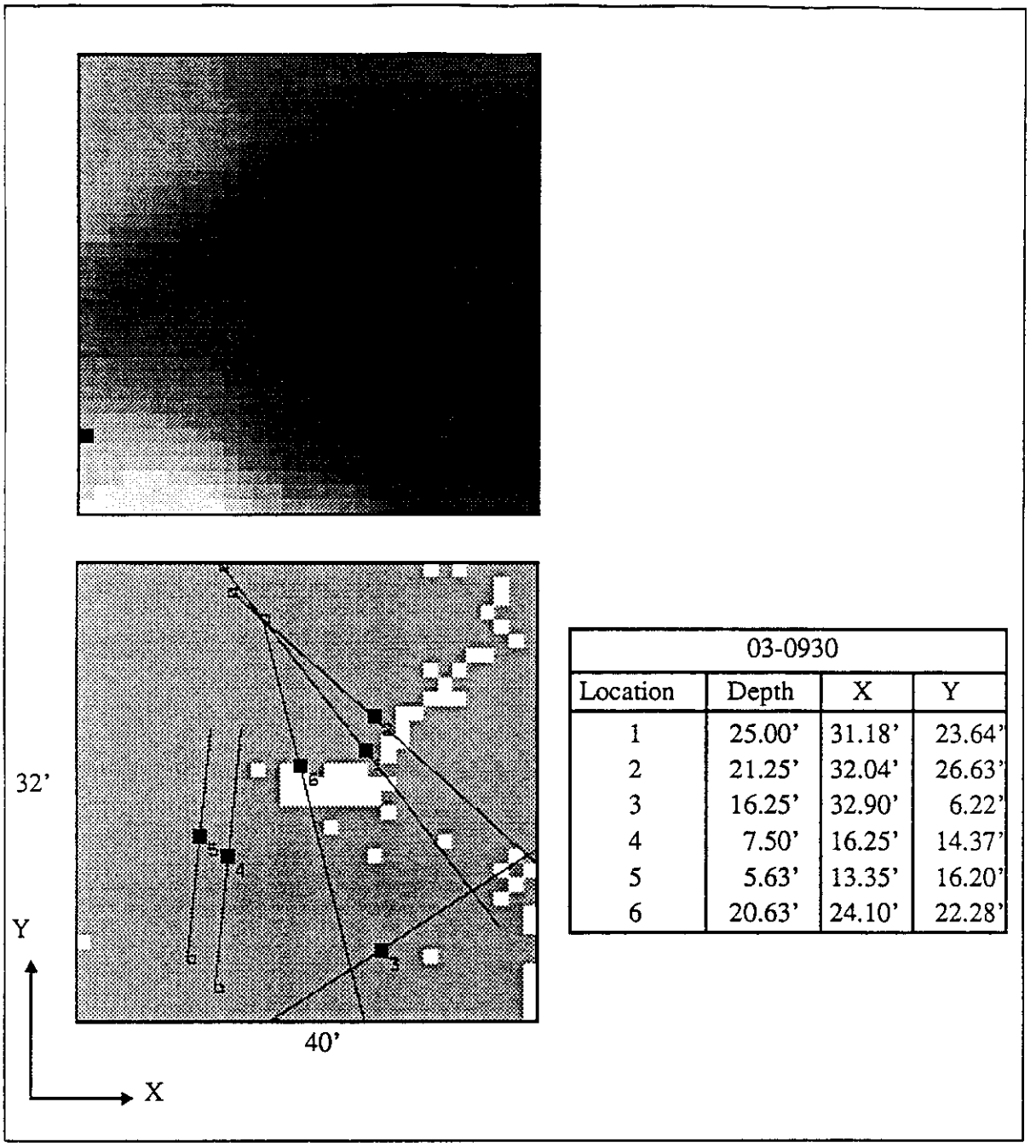

03-0930			
Location	Depth	X	Y
1	25.00'	31.18'	23.64'
2	21.25'	32.04'	26.63'
3	16.25'	32.90'	6.22'
4	7.50'	16.25'	14.37'
5	5.63'	13.35'	16.20'
6	20.63'	24.10'	22.28'

Figure 5. Single Map at the Oliver Avenue Site

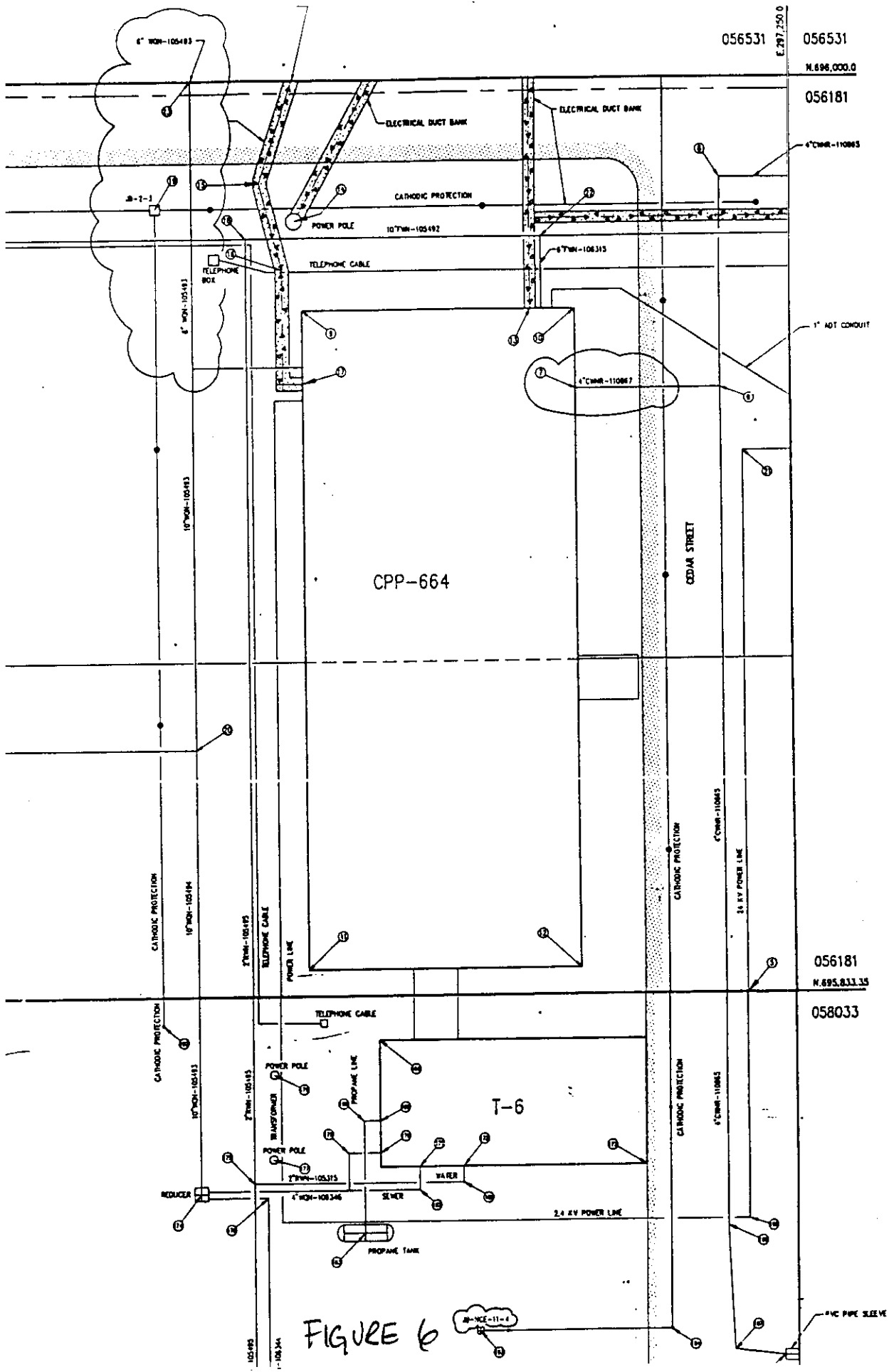

NOTES:

1. ALL ELEVATIONS BASED
2. ALL ELEVATIONS ARE T UNLESS OTHERWISE NO
3. FOR COMPLETE LEGEND
4. FEATURES WITHOUT SUR ARE SHOWN AT APPRO

FIGURE 6

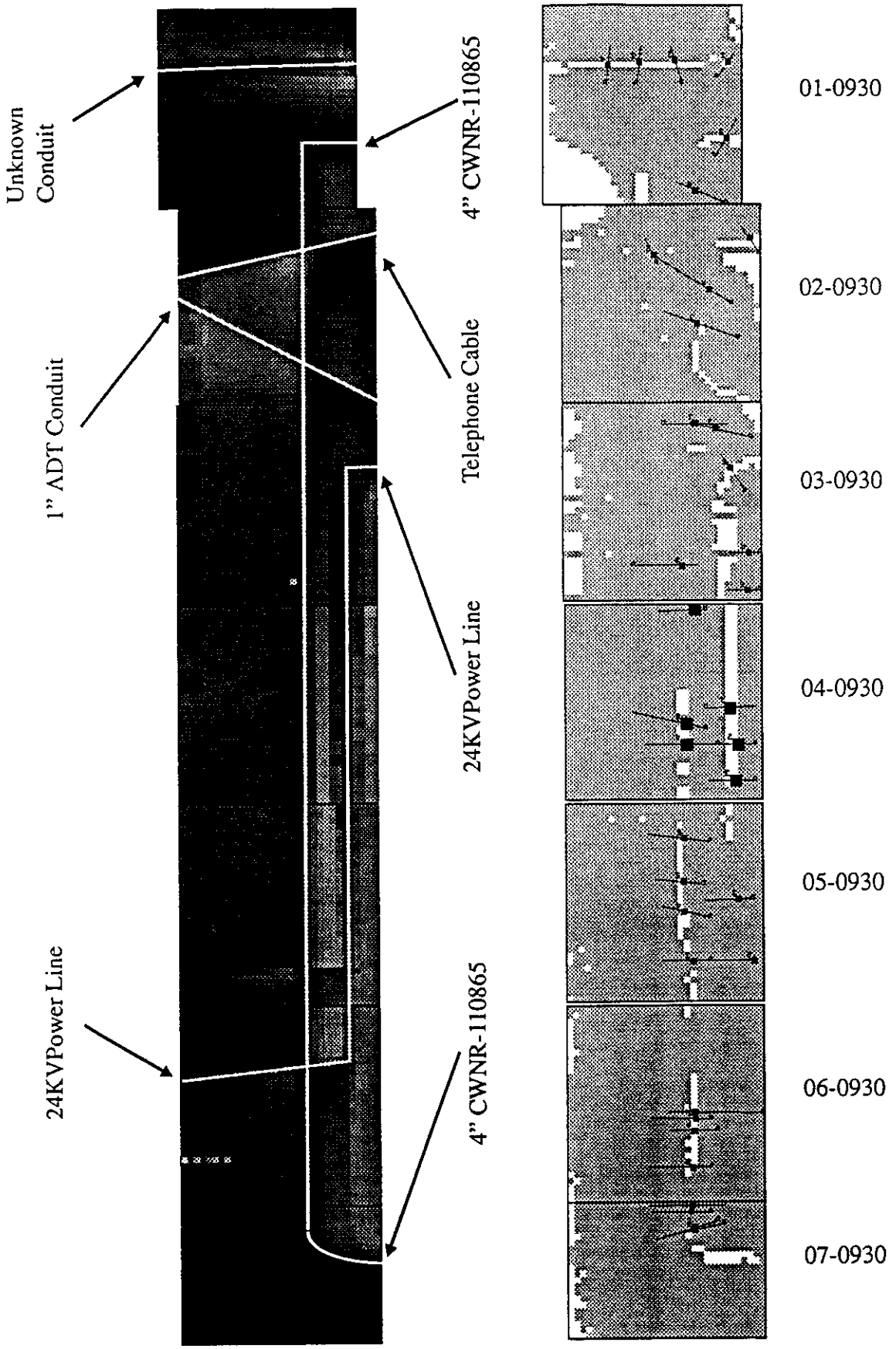

Figure 7. Collage of Maps & Sample Lines 1 thru 7 at Cedar Street Site (Not to Scale)

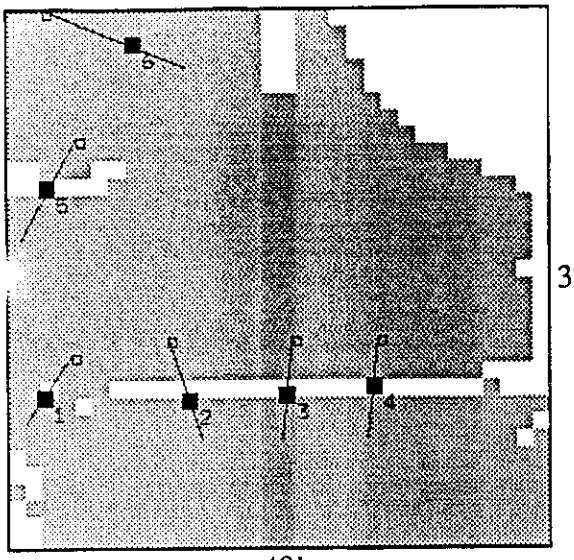

01-0930			
Location	Depth	X	Y
1	3.56'	3.48'	11.35'
2	4.56'	16.75"	11.06'
3	5.75'	25.72'	11.39'
4	5.19'	33.62'	12.08'
5	4.88'	3.85'	26.79'
6	6.31'	11.77'	37.39'

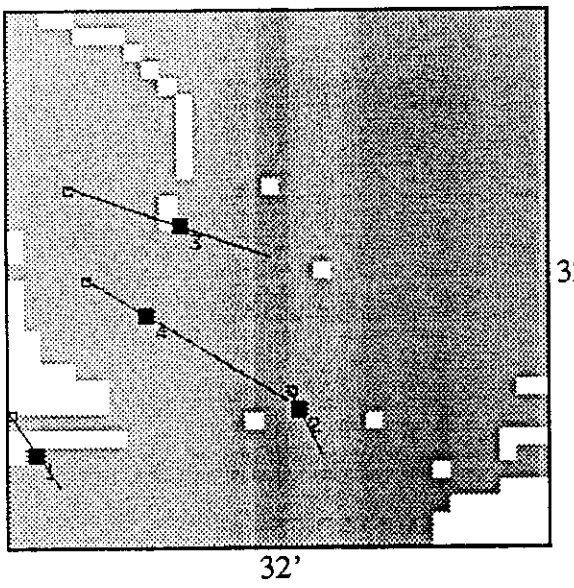

02-0930			
Location	Depth	X	Y
1	2.80'	1.67'	5.59'
2	1.00'	16.04'	8.29'
3	6.50'	9.58'	19.24'
4	7.50'	7.75'	13.89'
5	-	-	-
6	-	-	-

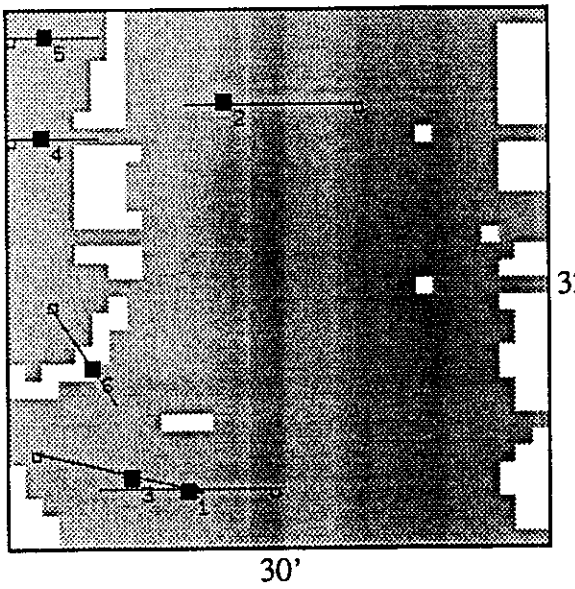

03-0930			
Location	Depth	X	Y
1	6.09'	9.32'	3.28'
2	6.00'	11.25'	24.85'
3	5.06'	6.45'	4.03'
4	0.84'	1.89'	22.96'
5	0.98'	2.02'	28.58'
6	1.50'	4.41'	10.04'

Figure 8. Maps 1 thru 3 at Cedar Street Site (Origin left bottom corner, Not to Scale)

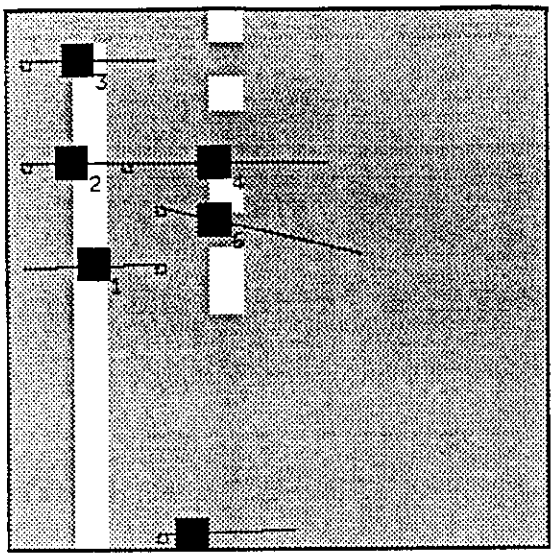

32'

30'

04-0930			
Location	Depth	X	Y
1	3.47'	4.57'	15.94'
2	2.81'	3.66'	21.57'
3	3.47'	3.86'	27.19'
4	6.28'	10.89'	21.57'
5	6.28'	9.58'	0.87'
6	5.91'	10.83'	18.38'

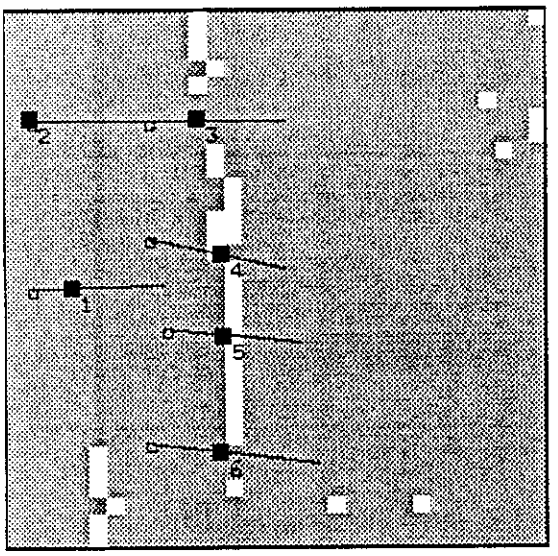

32'

30'

05-0930			
Location	Depth	X	Y
1	1.59'	3.51'	14.51'
2	1.59'	1.32'	23.94'
3	4.88'	10.10'	23.91'
4	4.97'	11.31'	16.32'
5	5.30'	11.41'	11.77'
6	6.94'	11.17'	5.25'

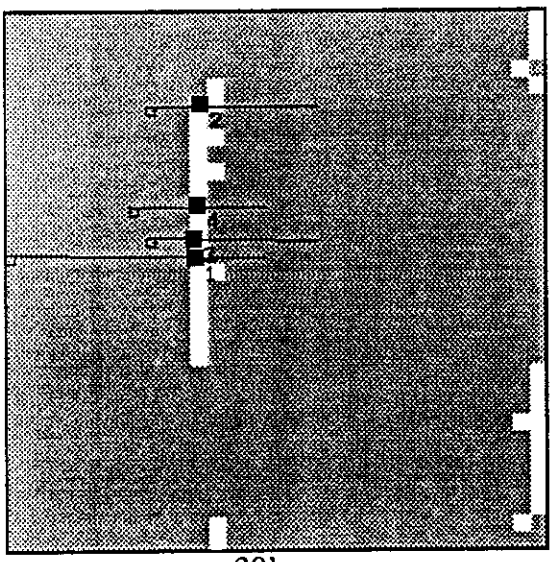

96'

30'

06-0930			
Location	Depth	X	Y
1	5.58'	9.97'	49.14'
2	5.20'	10.23'	74.55'
3	5.44'	9.89'	52.05'
4	5.44'	10.11'	57.66'
5	-	-	-
6	-	-	-

Figure 9. Maps 4 thru 6 at Cedar Street Site (Origin left bottom corner, Not to Scale)

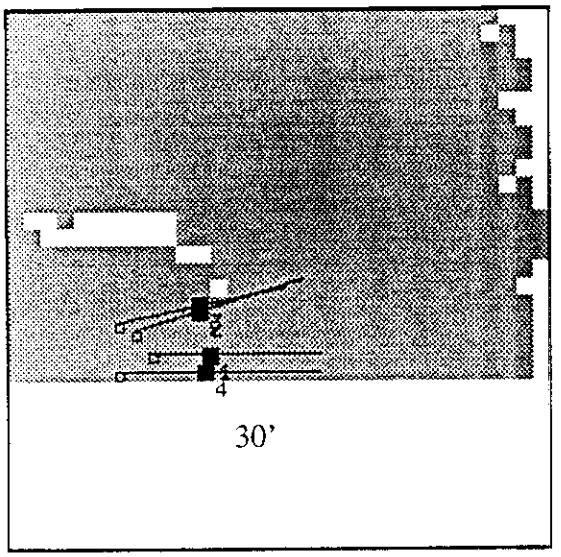

07-0930			
Location	Depth	X	Y
1	4.69'	10.54'	1.41'
2	4.78'	10.04'	3.92'
3	4.78'	10.09'	4.22'
4	5.30'	10.28'	0.47'
5	-	-	-
6	-	-	-

Figure 10. Map 7 at Cedar Street (Origin left bottom corner, Not to Scale)

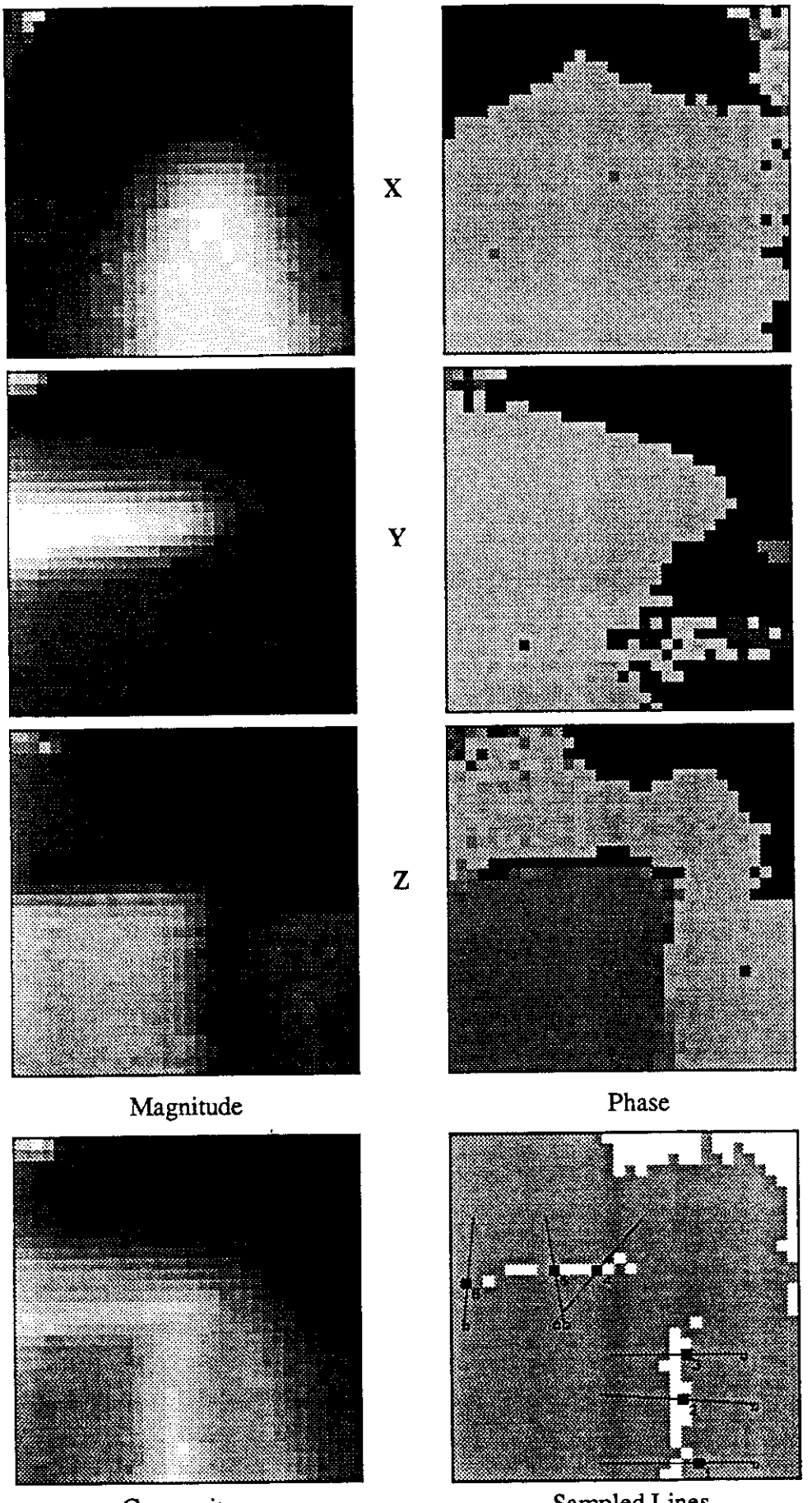

Figure 11. Digitized Magnetic Map of case 01-0927

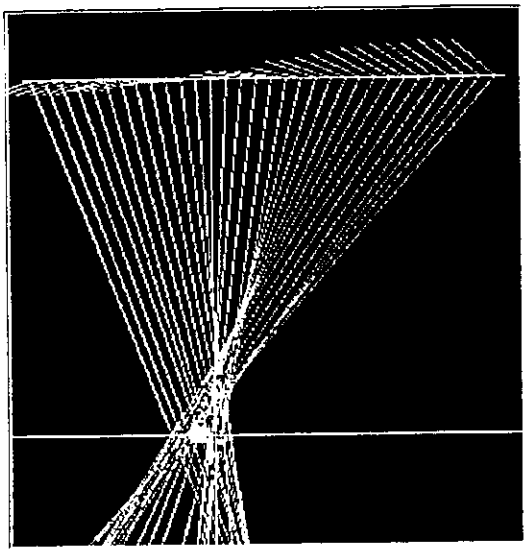

1

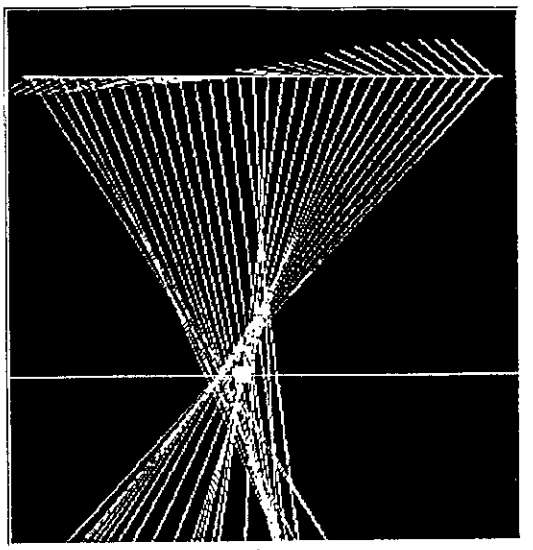

2

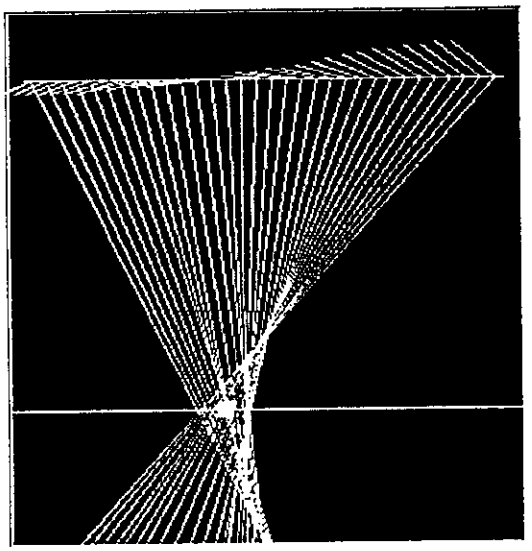

3

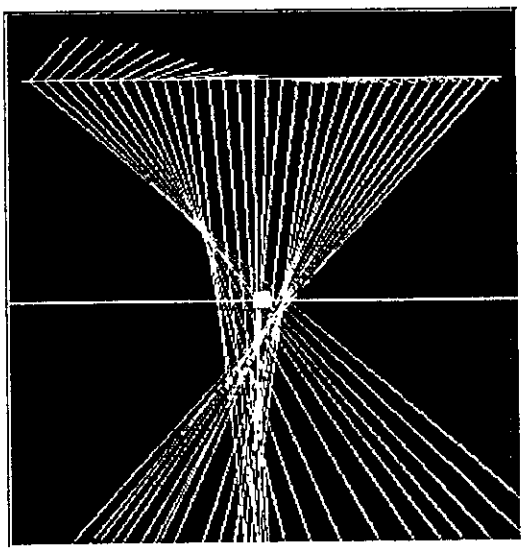

4

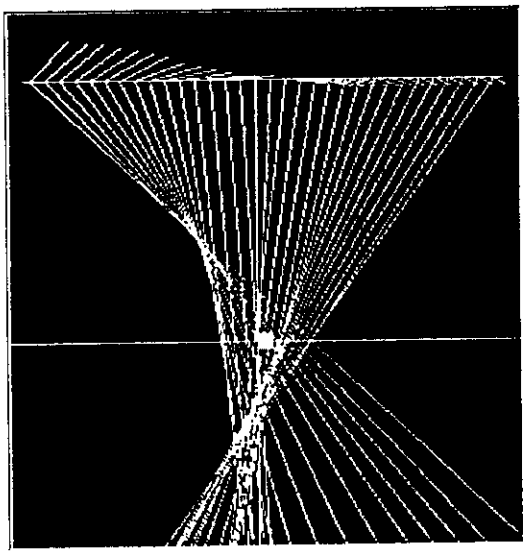

5

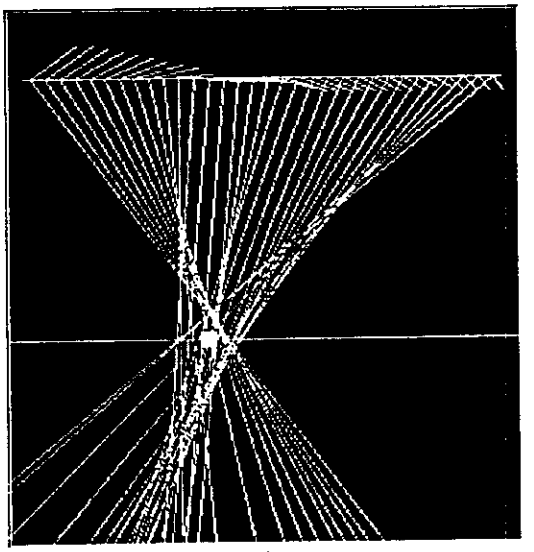

6

Figure 12. Field and Depth Vectors for Case 01-0927

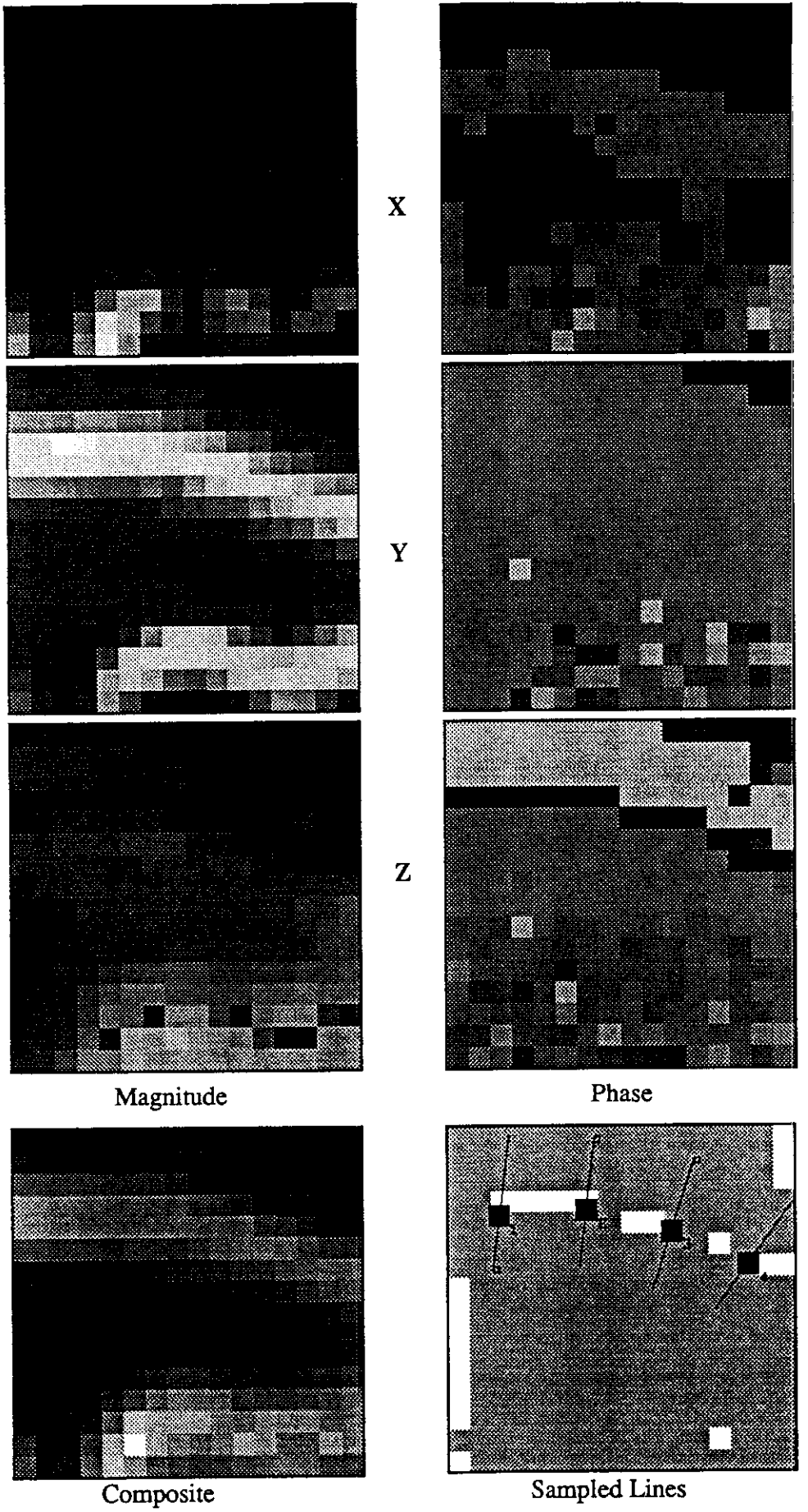

Figure 13. Digitized Magnetic Map of case 02-0927

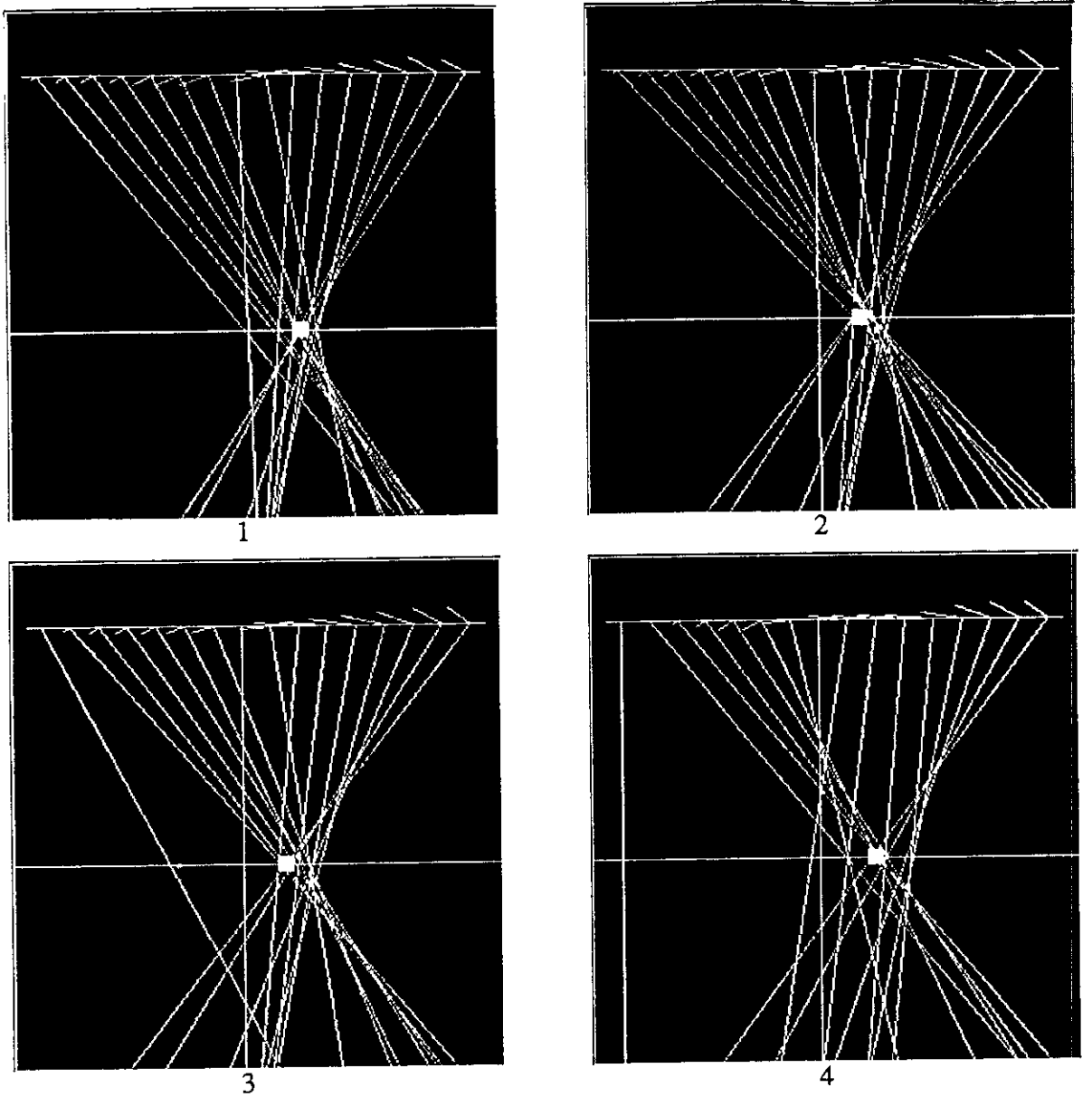

Figure 14. Field and Depth Vectors for Case 02-0927

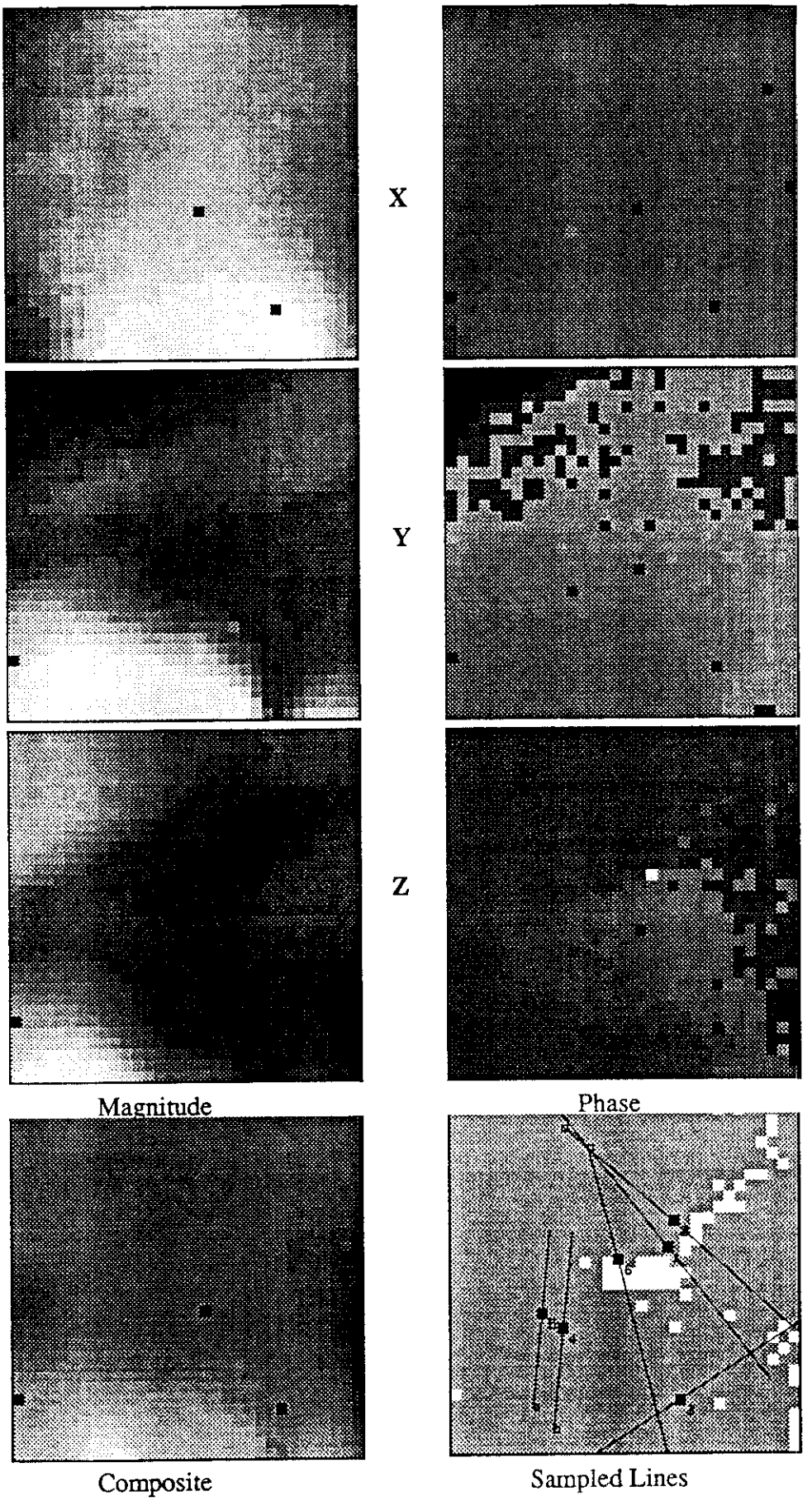

Figure 15. Digitized Magnetic Map of case 03-0927

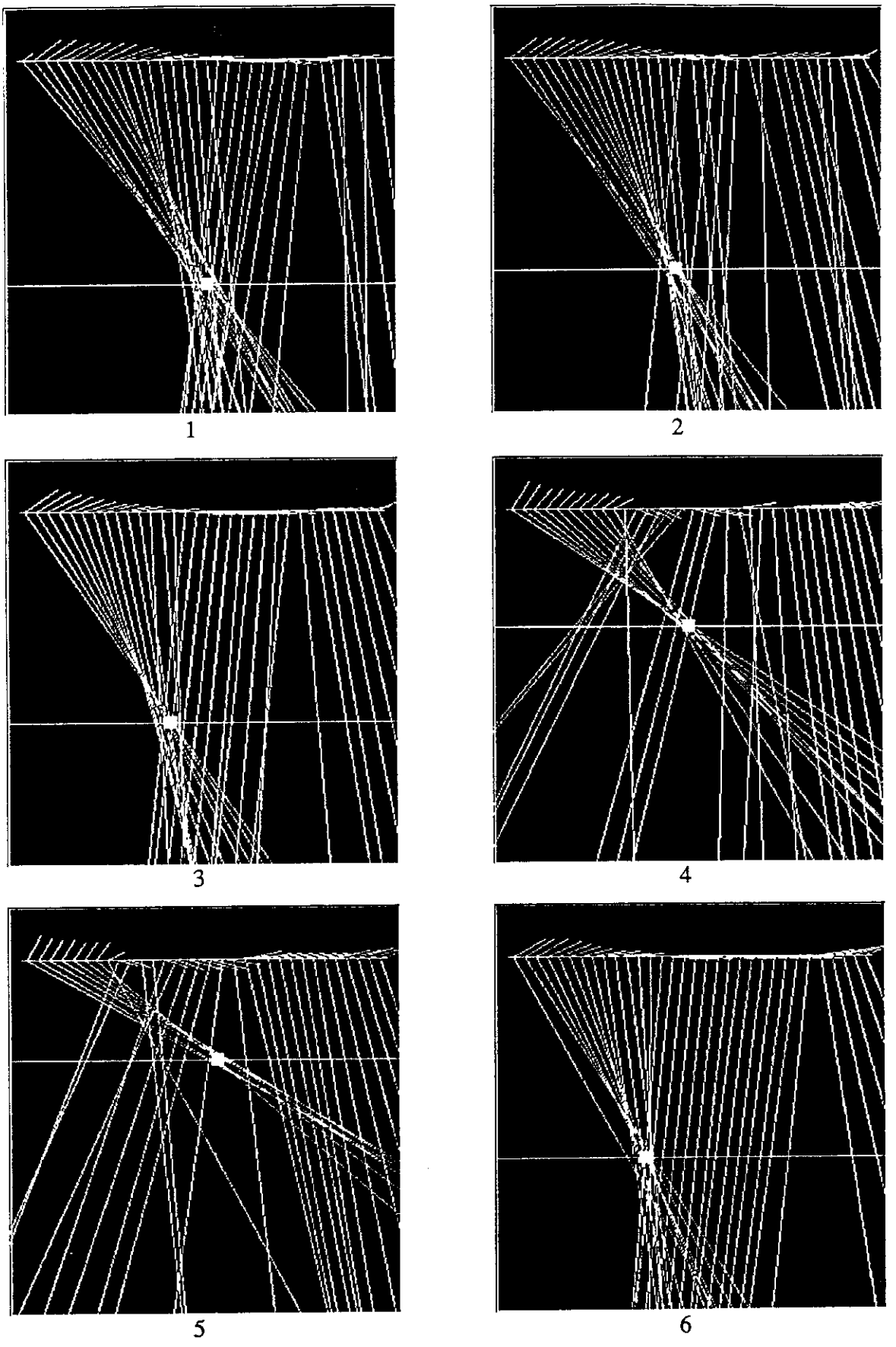

Figure 16. Field and Depth Vectors for Case 03-0927

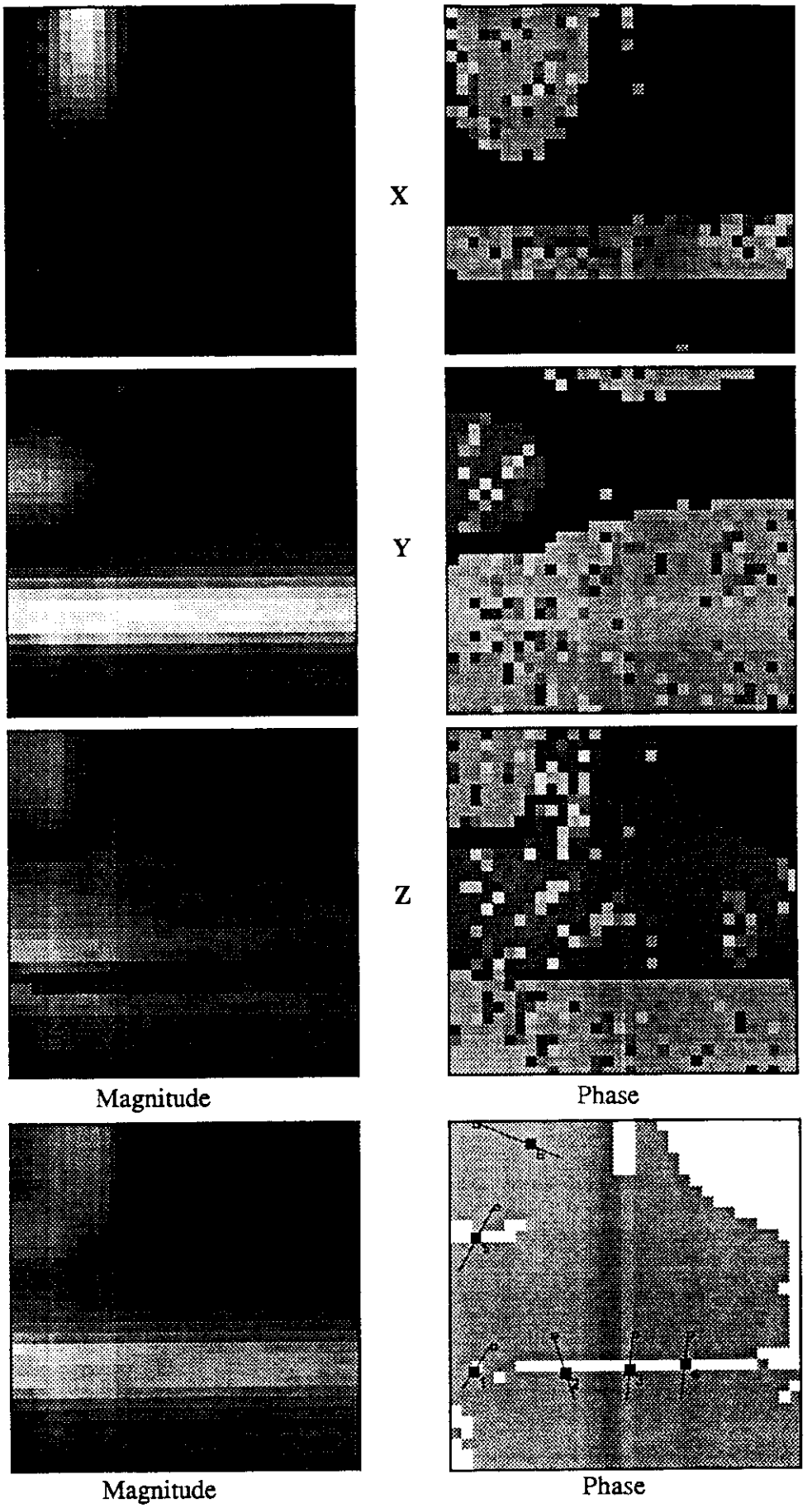

Figure 17. Digitized Magnetic Map of case 01-0930

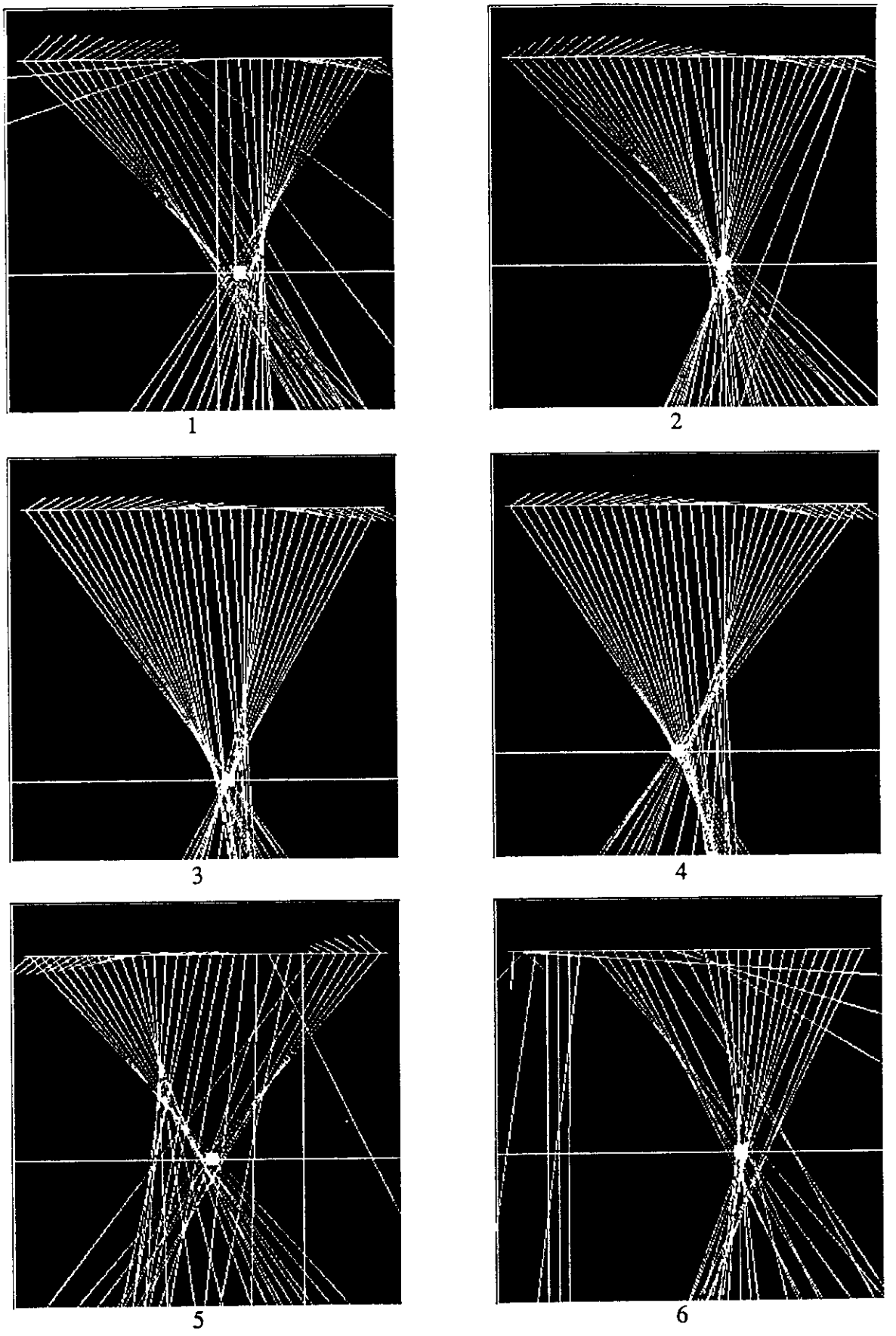

Figure 18. Field and Depth Vectors for Case 01-0930

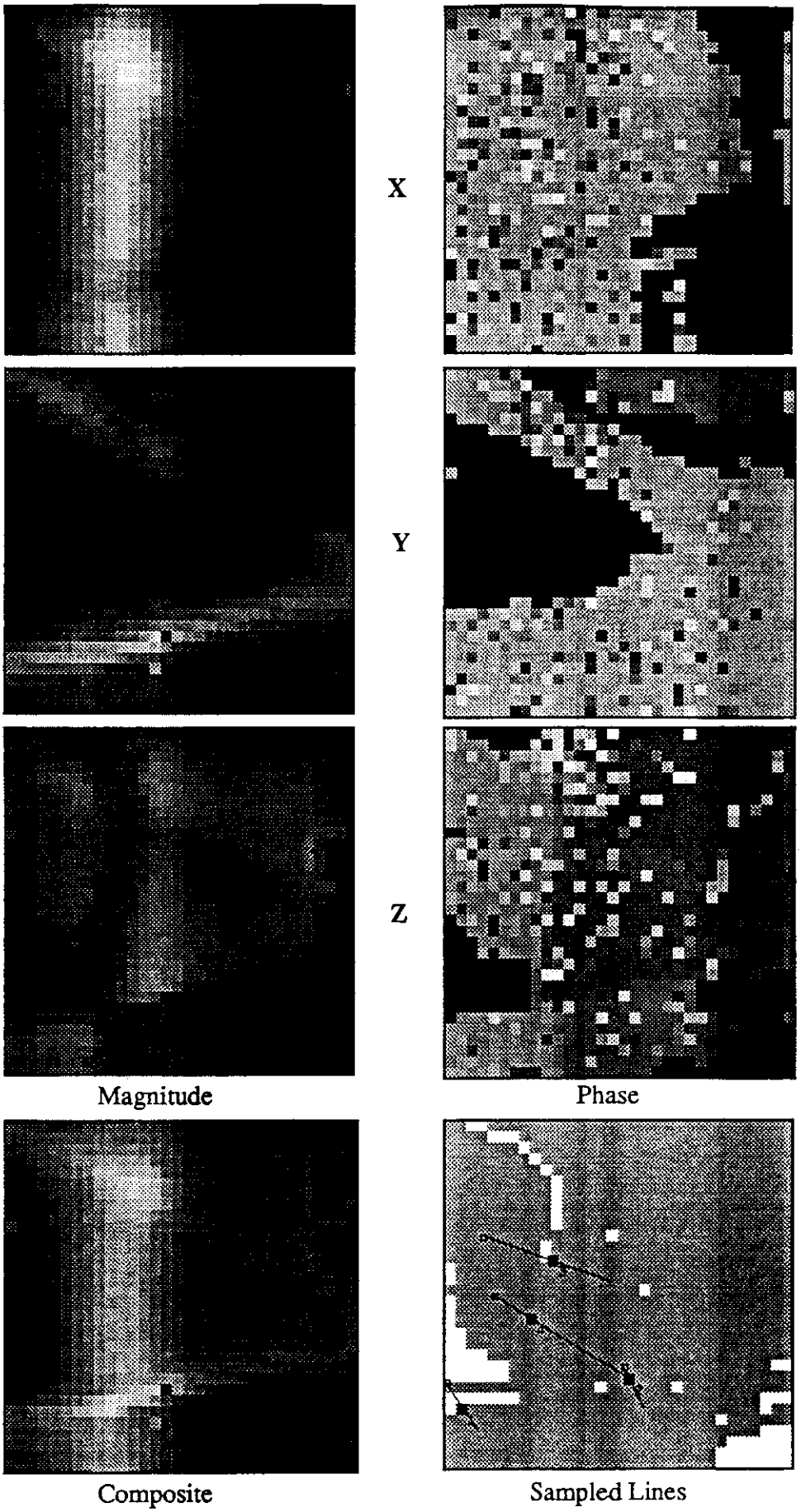

Figure 19. Digitized Magnetic Map of case 02-0930

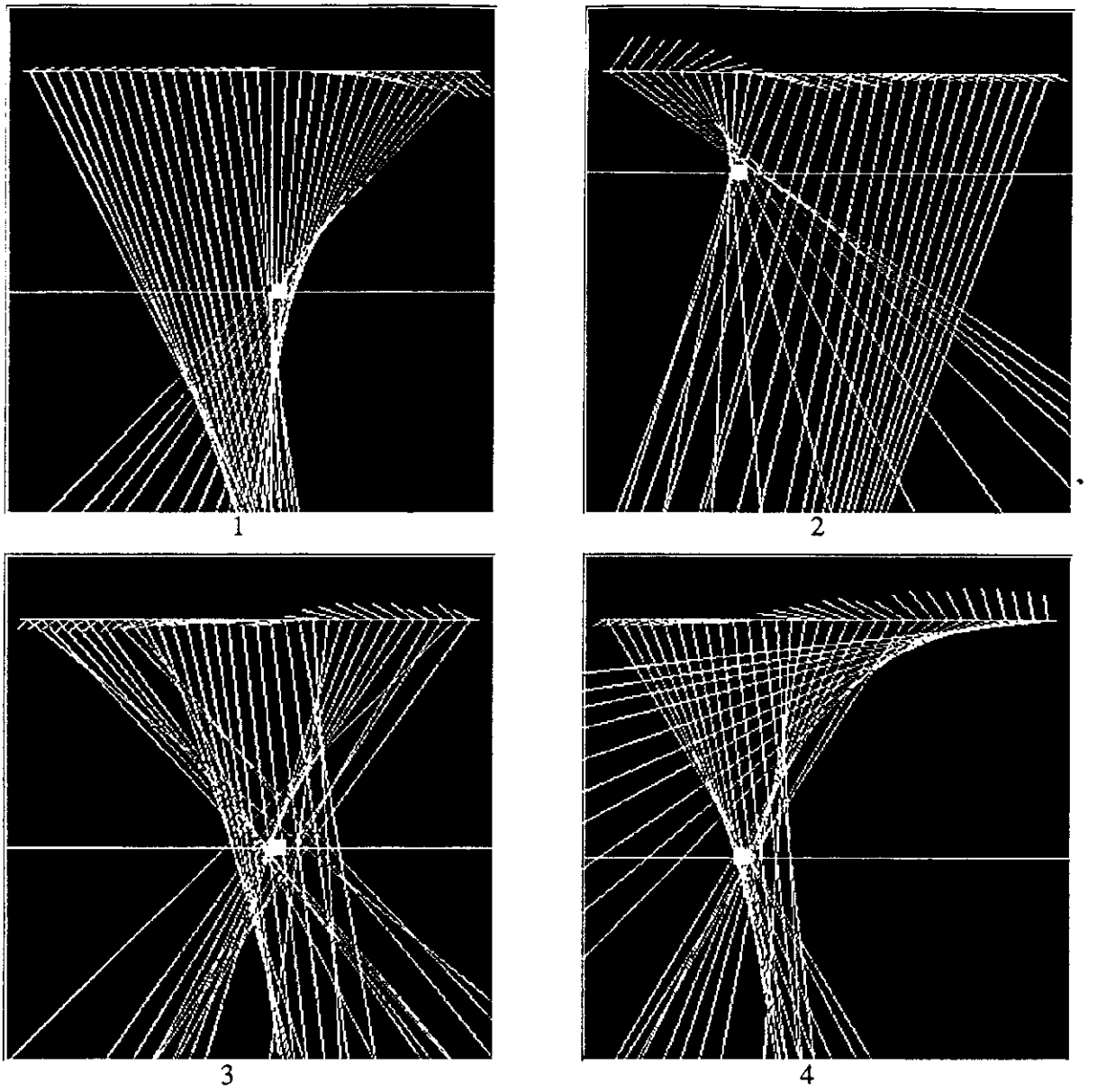

Figure 20. Field and Depth Vectors for Case 02-0930

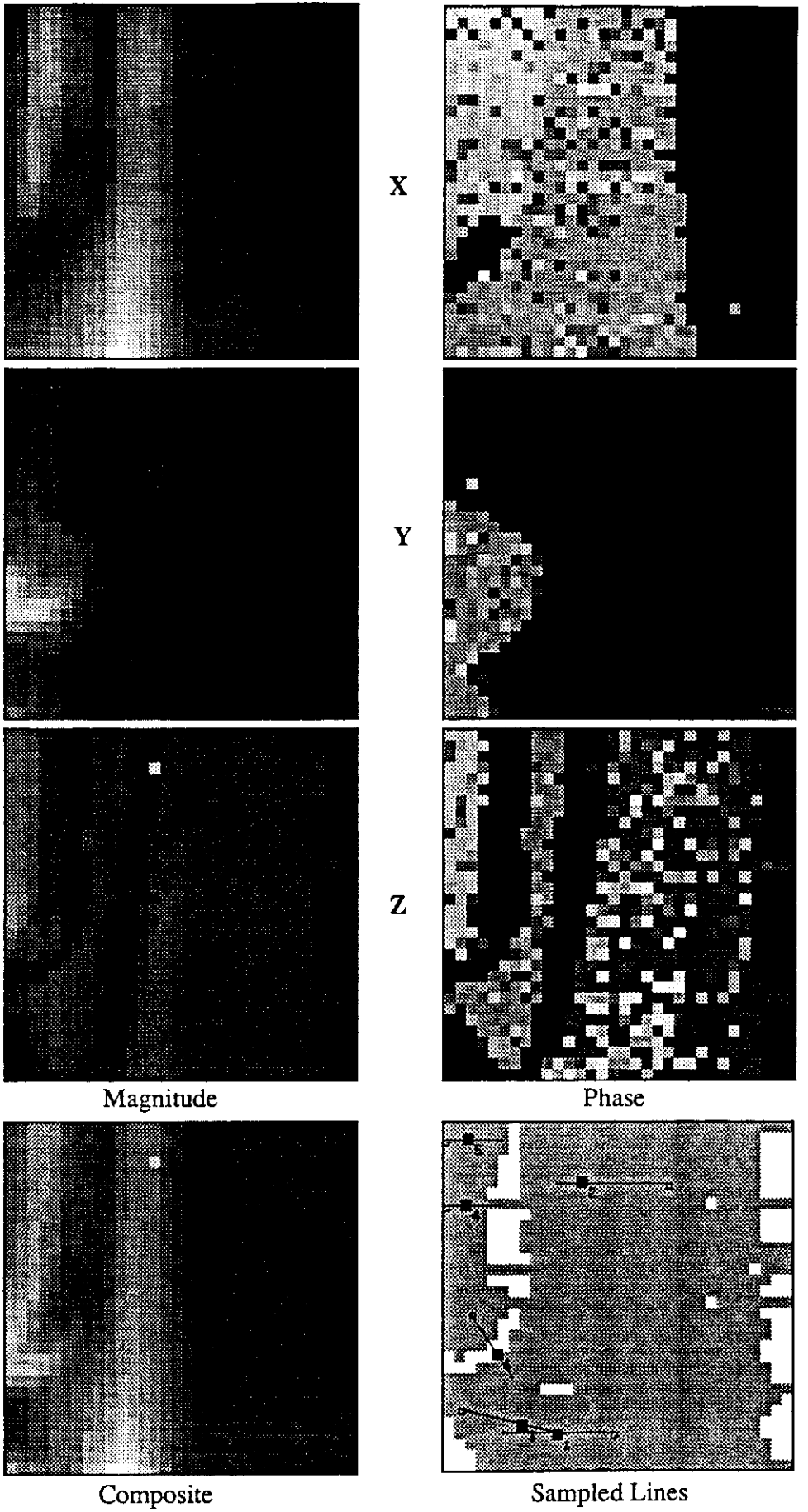

Figure 21. Digitized Magnetic Map of case 03-0930

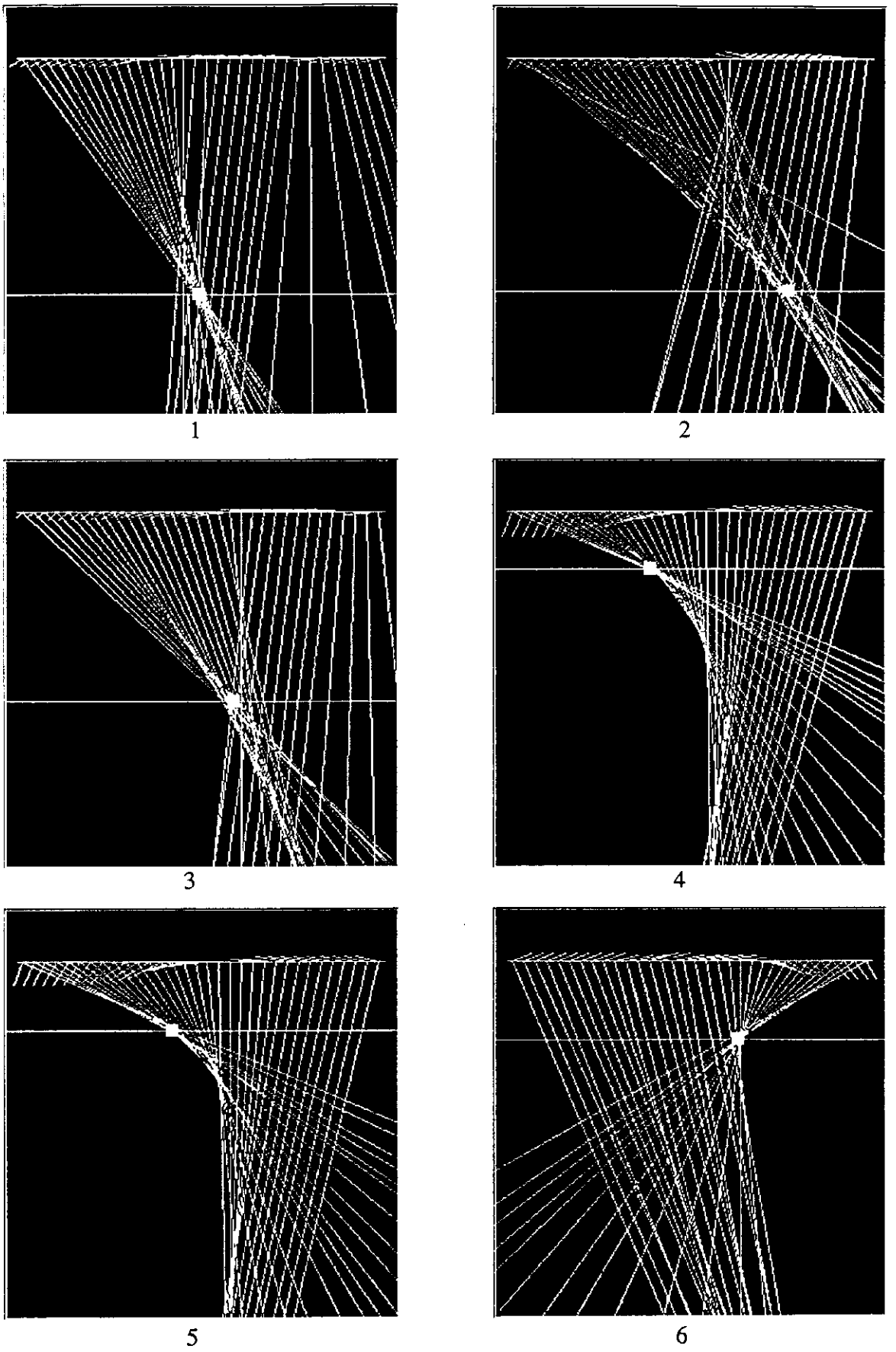

Figure 22. Field and Depth Vectors for Case 03-0930

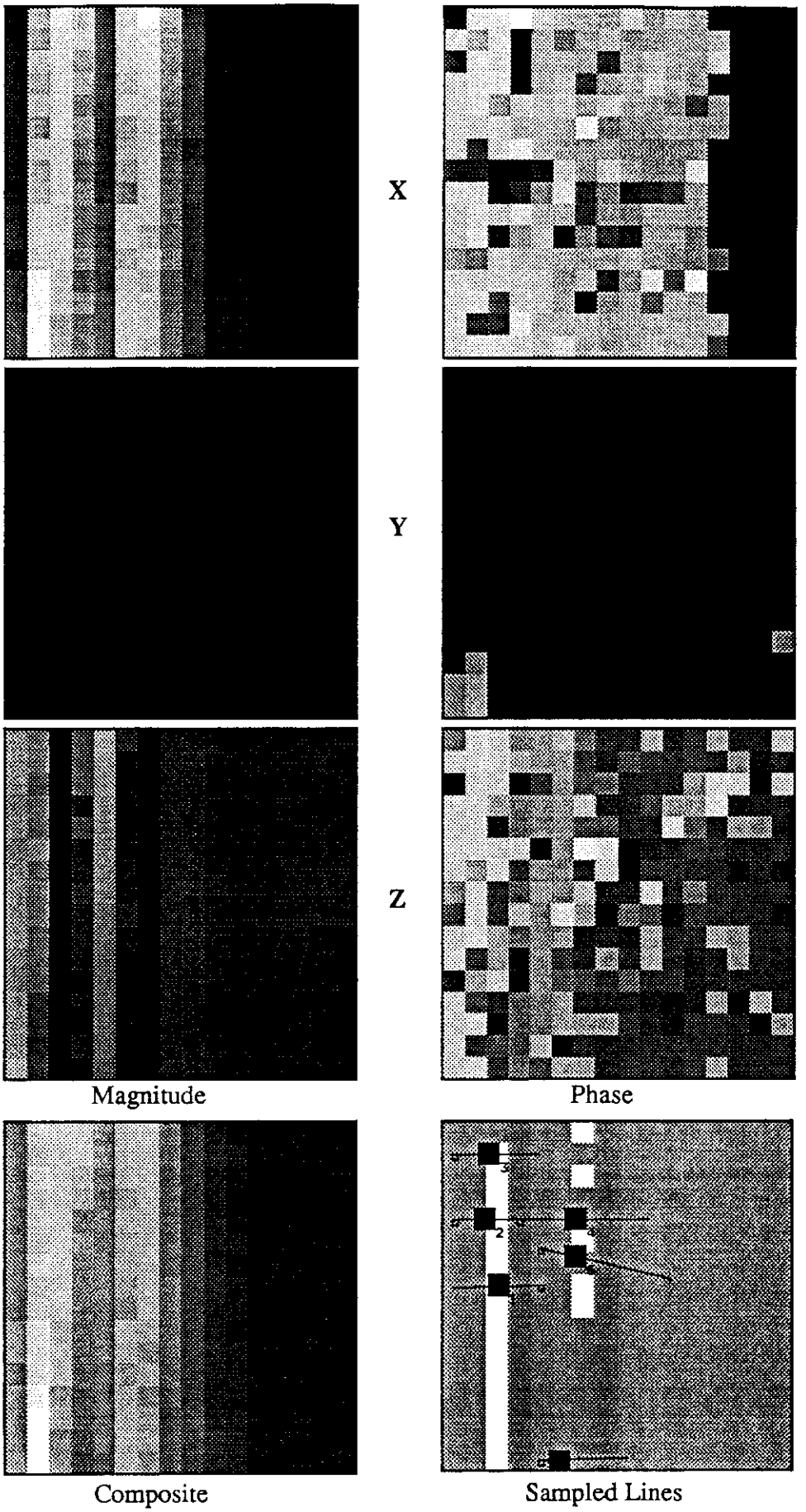

Figure 23. Digitized Magnetic Map of case 04-0930

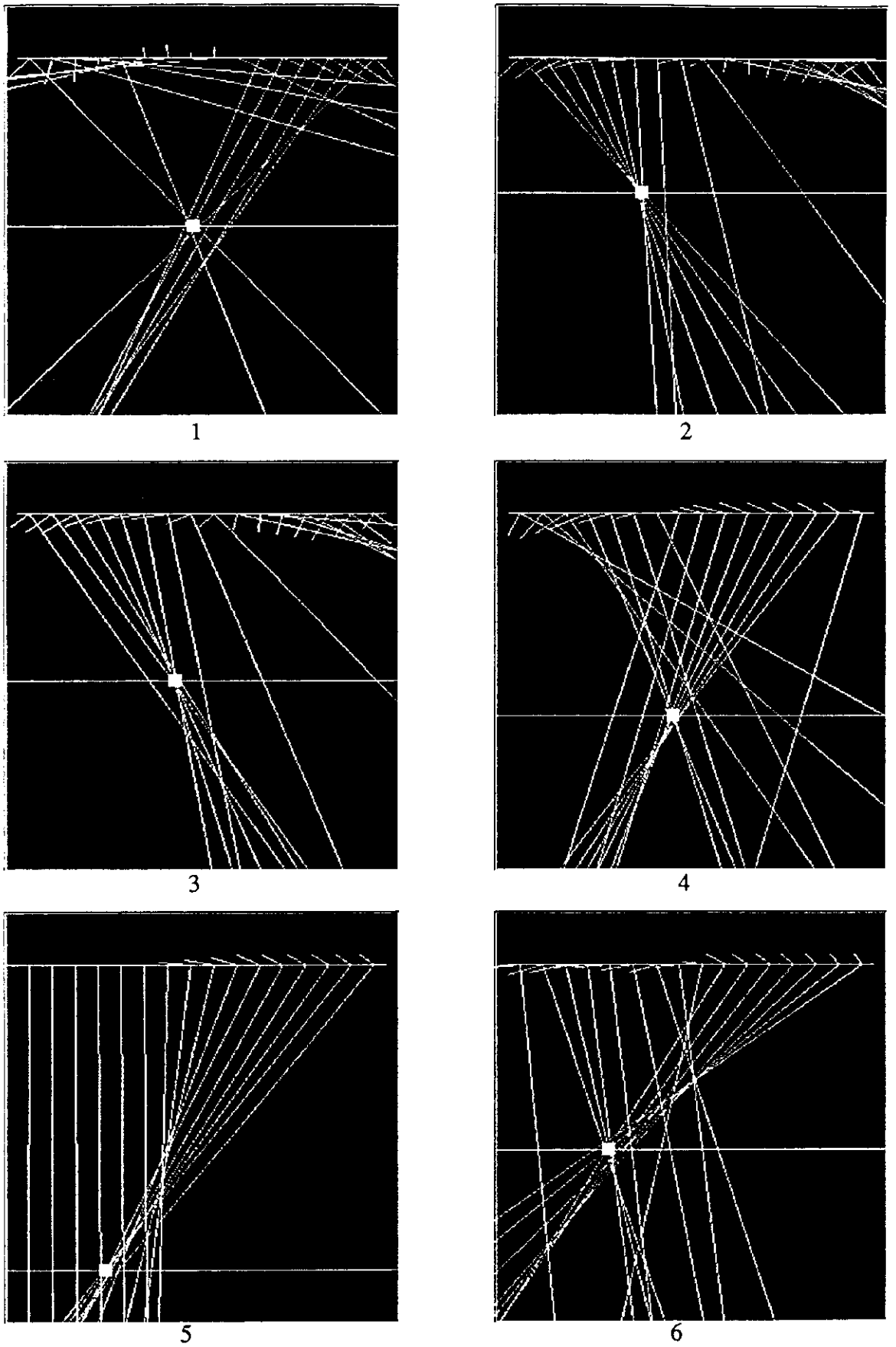

Figure 24. Field and Depth Vectors for Case 04-0930

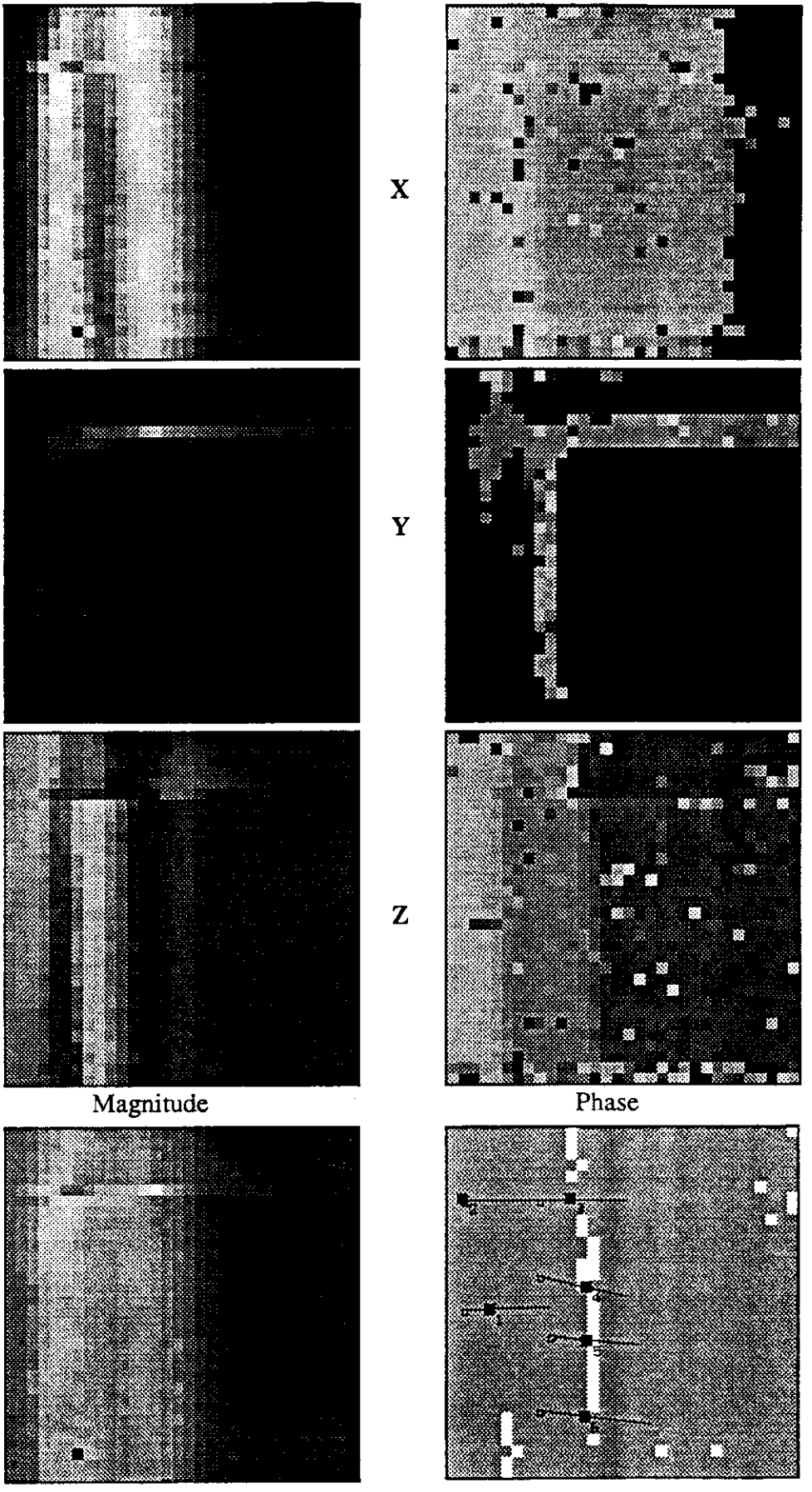

Figure 25. Digitized Magnetic Map of case 05-0930

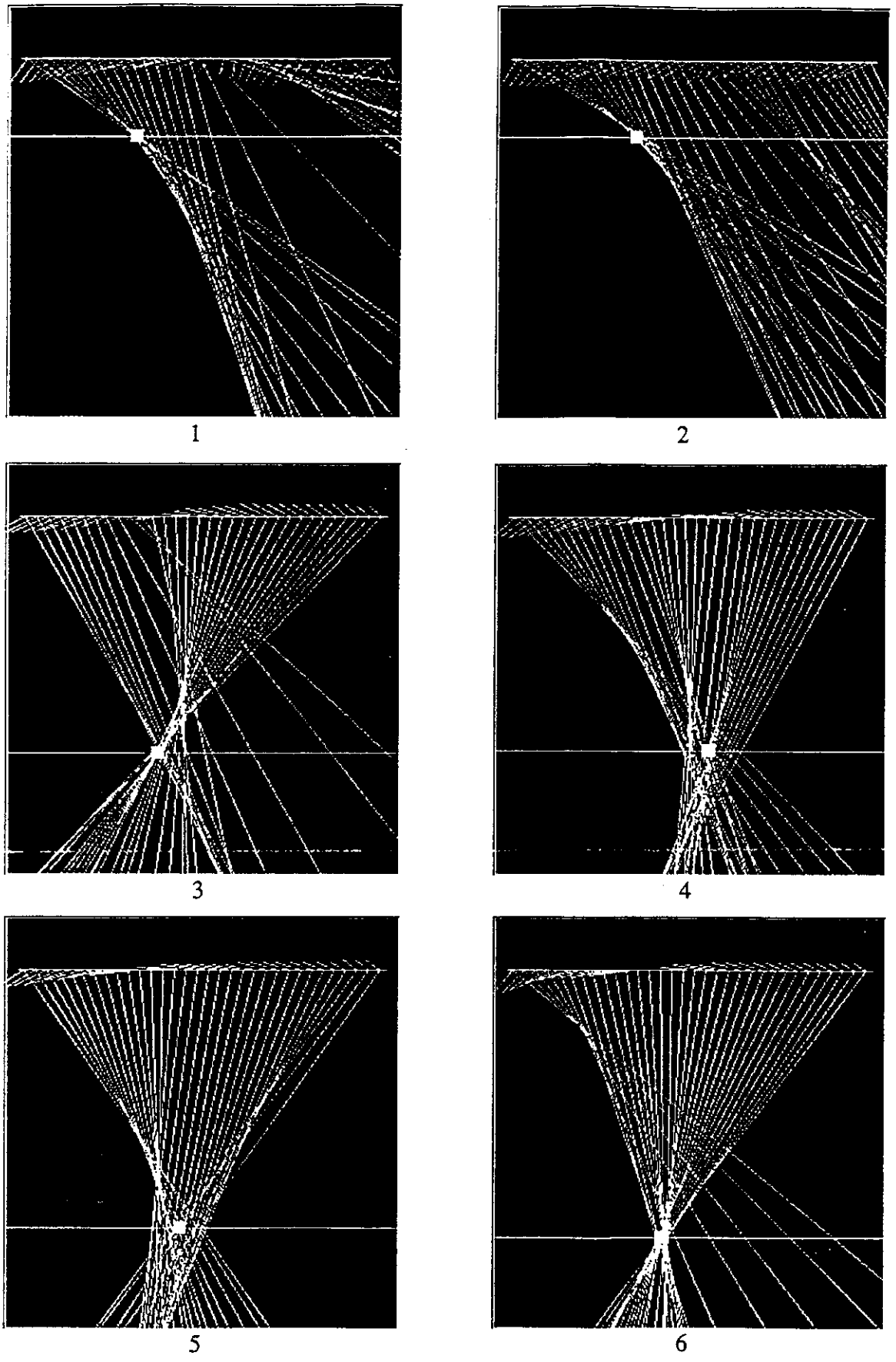

Figure 26. Field and Depth Vectors for Case 05-0930

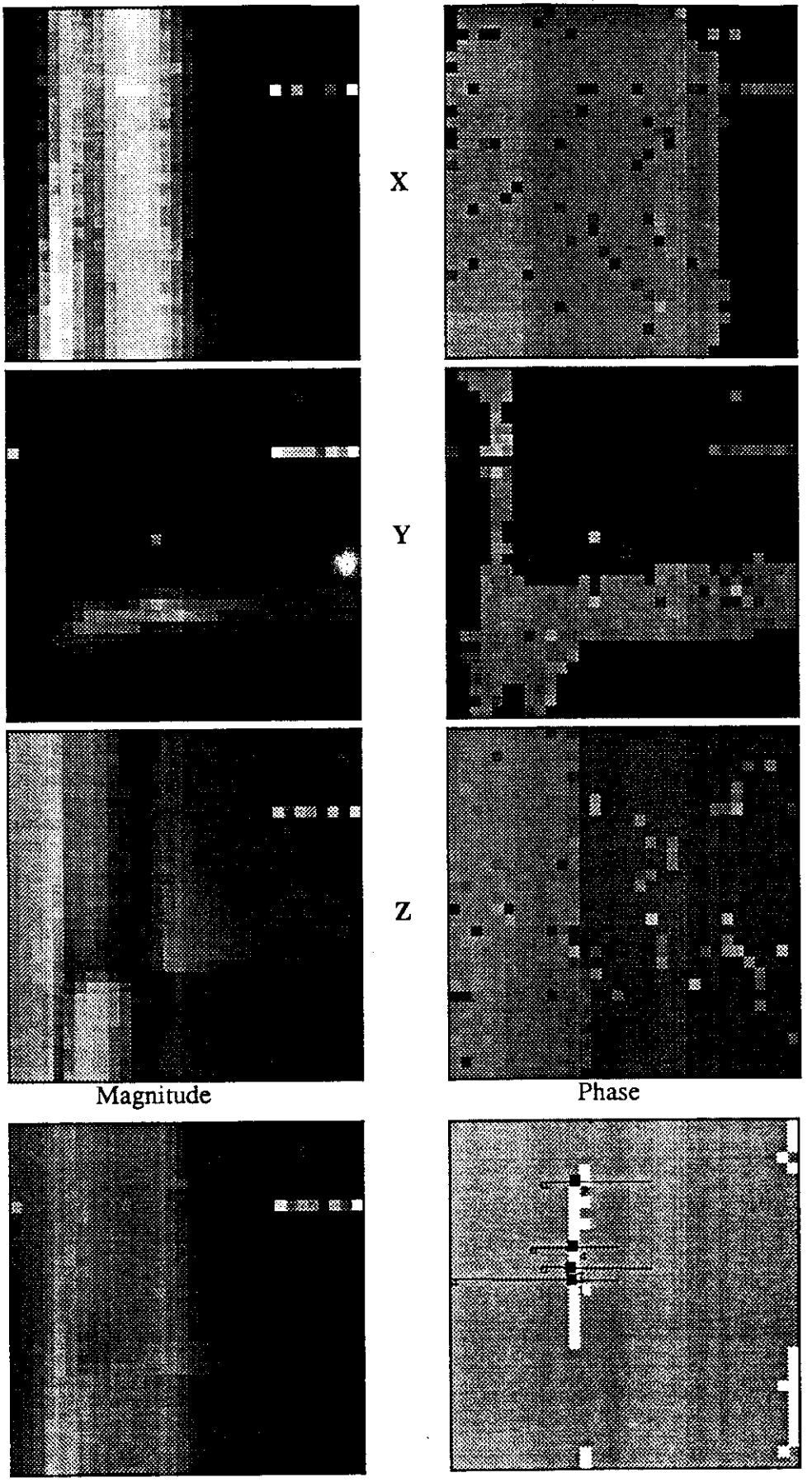

Figure 27. Digitized Magnetic Map of case 06-0930

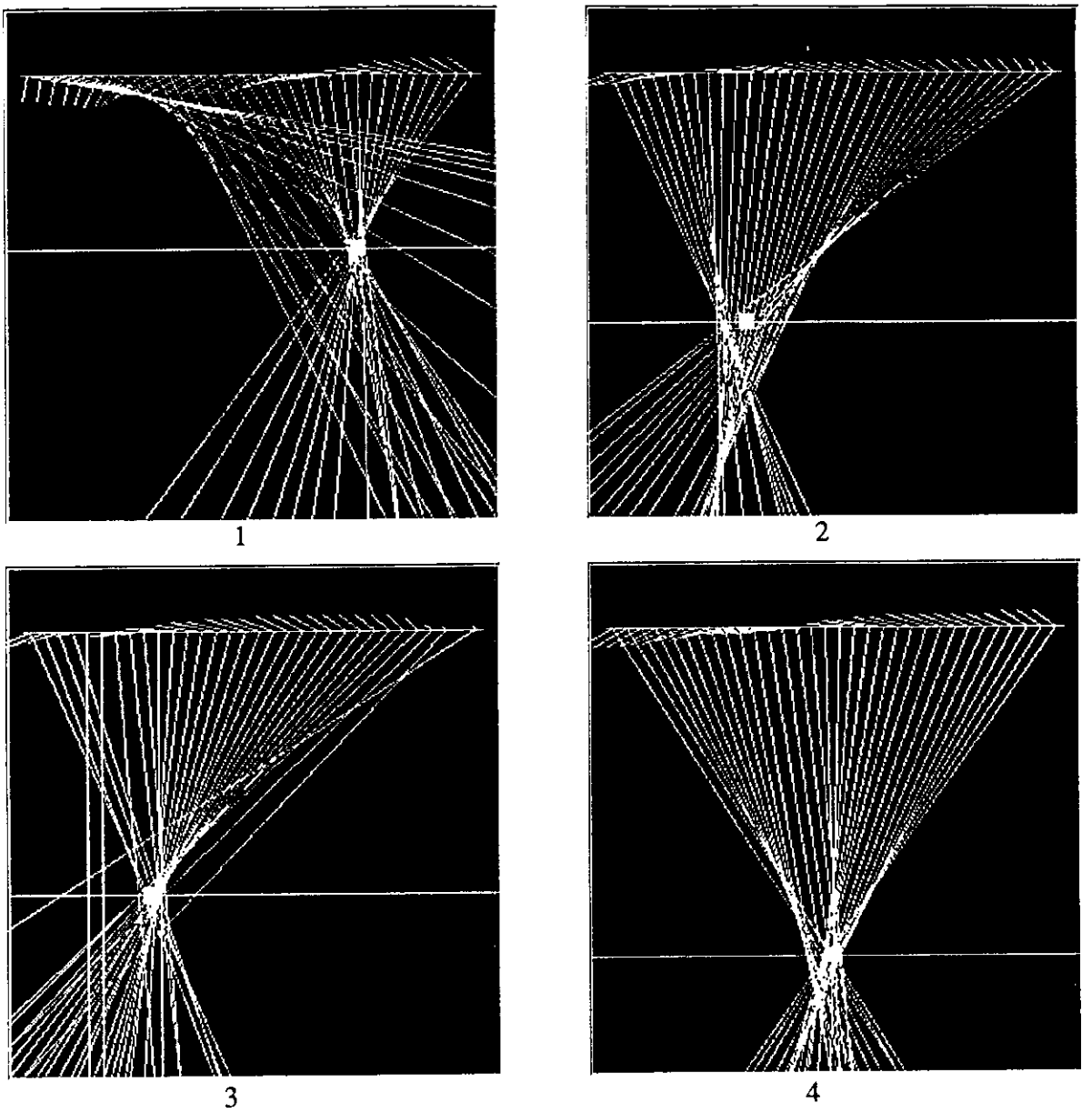

Figure 28. Field and Depth Vectors for Case 06-0930

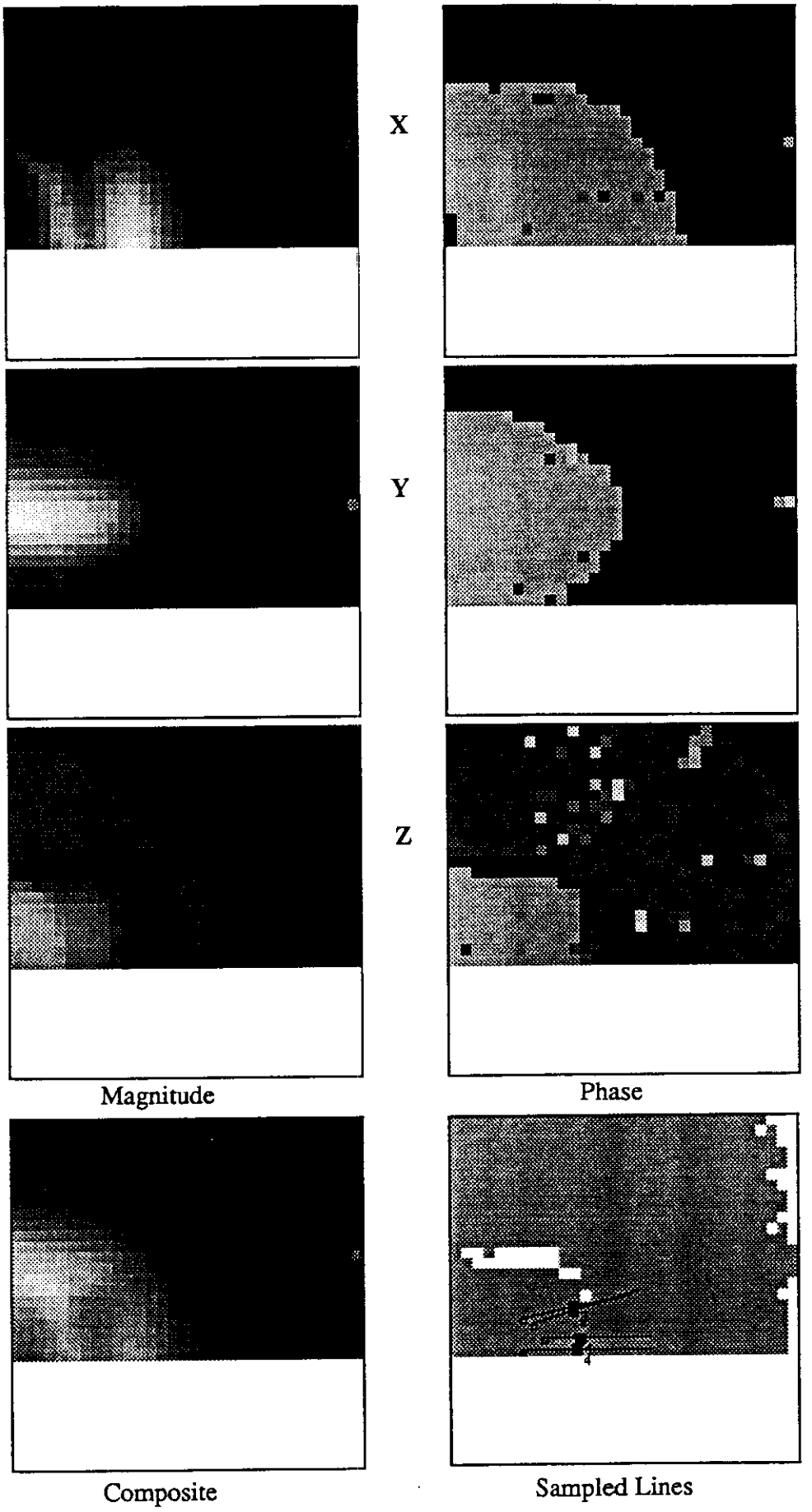

Figure 29. Digitized Magnetic Map of case 07-0930

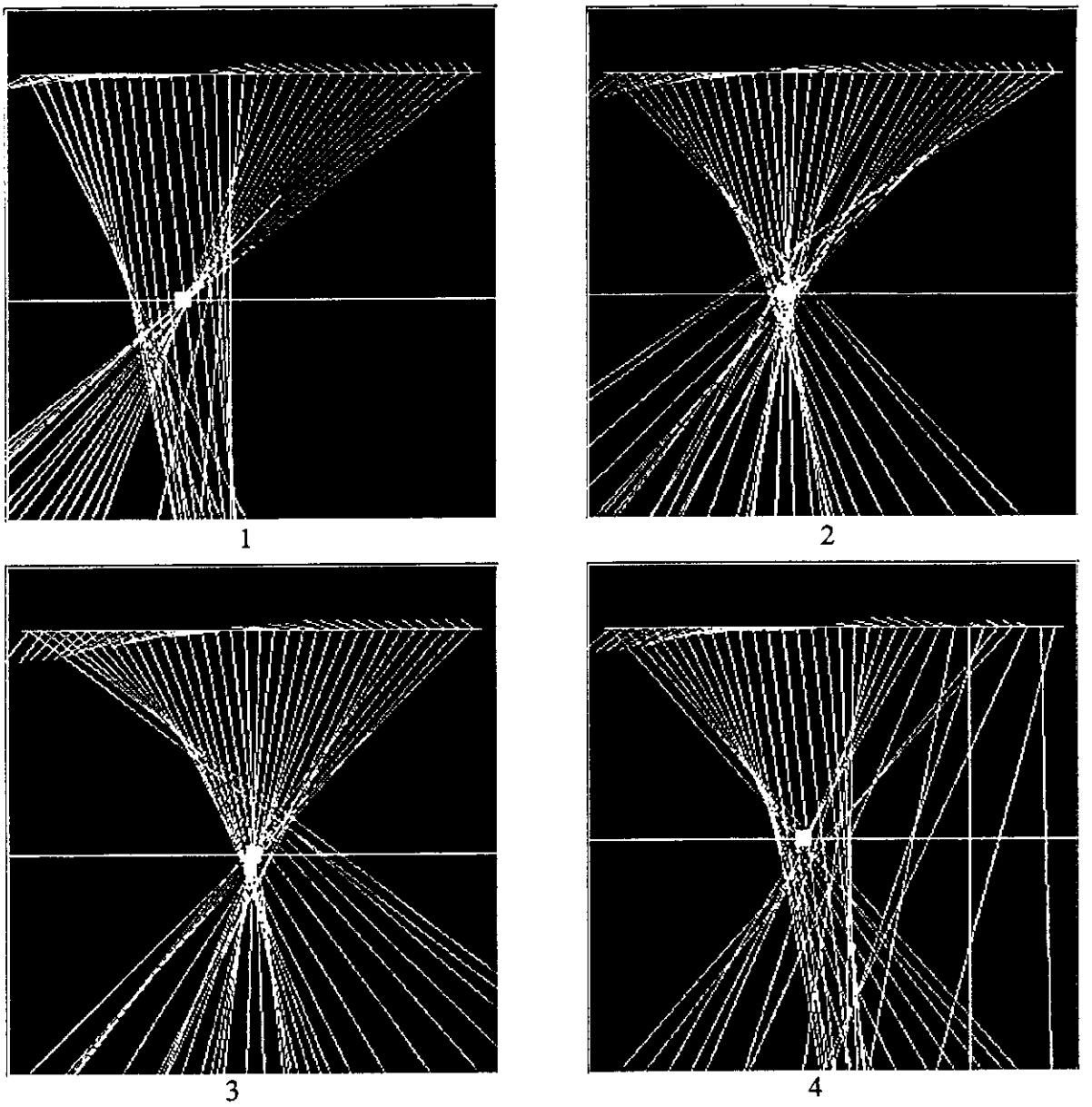

Figure 30. Field and Depth Vectors for Case 07-0930